# Tailorable optical trap with Digital Micromirror Device for Dysprosium experiment

Thibault BOURGEOIS

**Physikalisches Institut**
Universität Heidelberg

Quantum Fluids Group

under the supervision of
**Prof. Dr. Lauriane Chomaz**

**Abstract**

This report presents a setup to create arbitrary potentials for trapping two-dimensional Bose Einstein Condensate of Dysprosium. They are created by modulating the amplitude of a 532nm laser beam using a Digital Micromirror Device. The algorithm to optimize these potentials is explained and the accuracy as well as the stability of the trap are characterized. Finally simulations of the condensate in the obtained flat top trap are conducted and the perturbations of the atomic density with respect to the parameters of the condensate are studied.

## Acknowledgments

First of all I would like to thank Prof. Lauriane Chomaz for welcoming me in your group and for your supervision, which is the best I could have hoped for.

Then I want also to thank Shuwei Jin for the time you took to understand my complicated programs and I wish you good luck to implement the final setup, you will need it for the alignment !

I will also never forget Jianshun for all the tips you gave me and for never losing hope even with my coupling efficiency of 1%, as well as Karthik for the good time at the street food festival even if the churros were maybe a little bit too much... I'm also waiting for you to show you Paris, it's not as bad as Charles says !

I thank also Charles for going with me through the nightmare of finding accommodation in Heidelberg, and we still need to visit the beautiful city of Kehl ! And thanks Sarah for your involvement in our French lectures : "Oui, Oui, baguette, croissant, trottoir, porte monnaie !"

Thanks also to Christian for making me discover the incredible sport of Kabaddi as well as the ~~existence of Bielefeld~~.

Finally, I would like to thank Britta for trying to understand how the french prépa system works even if as I say "it's complicated" and Maurice for trying to explain to me that e-scooter are maybe not evil !

Last but not least, I want to say a huge thank you to the Deutsche Bahn for allowing me to travel easily and punctually (if you measure time in day, they were always on time !) across Germany as well as showing me that you can sleep quite well in the bench of Karlsruhe train station when your train is canceled.

# Contents

# 1 Theoretical and technical background to the tailorable trapping of Dysprosium atoms

## 1.1 Dipolar atomic gases of Dysprosium

Before diving into the description of the experimental setup allowing to create tailorable traps, one should have an overview of the experiment in which it will fit. This experiment, built by the group of Lauriane Chomaz, is dedicated to the study of ultracold gases of Dysprosium atoms. They are of particular interest because the Dysprosium is the most magnetic atom, with a magnetic moment $\mu_m \simeq 10\mu_B$, where $\mu_B$ is the Bohr magneton. This moment causes a dipolar interaction [1] between atoms separated by a distance $r$ in the form of :

$$V_{dd}(\mathbf{r}) = \frac{\mu_0 \mu_m^2}{4\pi} \frac{1 - 3\cos^2\theta}{r^3} \tag{1}$$

where $\mu_0$ is the vacuum permeability and $\theta$ the angle defined in Figure 1.

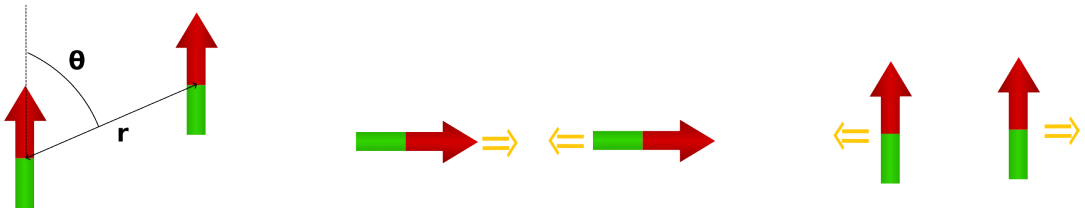


FIGURE 1 – Illustration of the dipolar interactions between two atoms. In the middle, we have the head to tail configuration and at the right, this is the side by side configuration.

This interaction is highly anisotropic. We see that for $\theta = 0$, a head to tail configuration, we have attractive interaction, while for $\theta = \frac{\pi}{2}$, a side by side configuration, the interaction is repulsive. This is shown in Figure 1.

Once they are cooled to very low temperatures, the atoms of mass $m$ turned into a Bose Einstein Condensate where a macroscopic number of atoms occupy the ground state of the system. However, unlike most of the cold atom gases, where the behavior of the condensate is determined by a kinetic term and some contact interaction between the atoms, described by a scattering length $a_s$, here the strong dipolar interactions adds a term in the Gross Pitaevskii equation for the evolution of the system [1, 2] :

$$i\hbar\frac{\partial\Psi}{\partial t} = \left[-\frac{\hbar^2}{2m}\nabla^2 + V(\overrightarrow{r}) + \frac{4\pi\hbar^2 a_s}{m}|\Psi|^2 + \frac{\mu_0\mu_m^2}{4\pi}\int \frac{1-3\cos^2\theta}{\|\overrightarrow{r}-\overrightarrow{r}'\|^3}|\Psi(\overrightarrow{r}')|^2 \mathrm{d}\overrightarrow{r}'\right]\Psi \tag{2}$$

where $\Psi$ is the macroscopic wavefunction of the system such that its norm is the square root of the atomic density and $\frac{\hbar}{m}\nabla\Phi$ is the velocity field with $\Phi$ the phase of $\Psi$ .

This long range dipolar interaction enables to observe new quantum states like supersolid [1] where the atom cloud displays superfluid properties as well as discrete translational symmetry like in a crystal and no longer the continuous one of (2) usually observed in superfluids. The goal now is to study this physics in 2D as well as the dynamics of for example vortices or turbulence in the atomic cloud. Being in 2D gives access to different transition mechanism like the Berezinskii-Kosterlitz-Thouless transition [3] and there might be other crystal structures than the ones observed in 3D.

The experiment is done in the science chamber shown in Figure 2 :

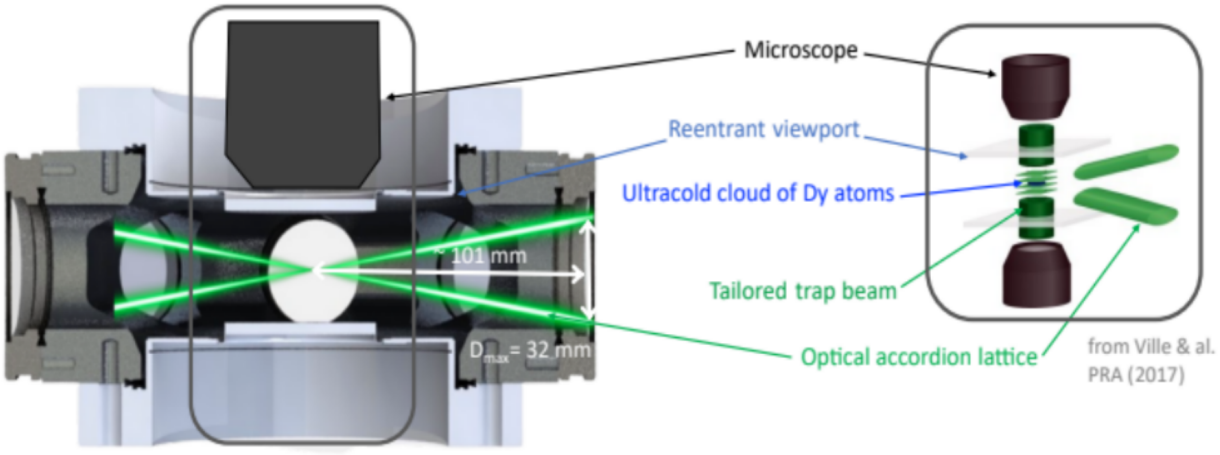


FIGURE 2 – Illustration of the science chamber of the main experiment. In addition of the accordion lattice beam represented coming from the side and the tailored beam from the top, there are six magneto-optical trap beams at 626nm and two beams at 1064nm for the crossed optical trap (adapted from seminar talk from L. Chomaz)

In this chamber, the atoms are loaded from a 3D magneto-optical trap [4] into a crossed optical dipole trap [5]. At this point, a Bose Einstein condensate was achieved in April 2023. In the future, the atoms will then be transferred in an accordion lattice trap [6] where they will be compressed into quasi-2D regime. Once they are in this 2D regime, we want to be able to trap them into different potentials and even time dependent ones to study their behavior and dynamics ; creating this tailorable optical trap is the topic of this report.

## 1.2 Optical trapping of Dysprosium

Like in any cold magnetic atoms experiment, the Dysprosium atoms are trapped using laser light [7]. Indeed light of intensity $I$ creates for atoms of polarizabilty $\alpha$ a potential $U = -\frac{1}{2\varepsilon_0 c} I \,\mathrm{Re}(\alpha)$ with $\varepsilon_0$ the vacuum permittivity and $c$ the speed of light. Since the Dysprosium ground state has a non zero angular momentum $J = 8$ and $m_J = -8$, it must be considered as an anisotropic medium and hence the polarizability must be decomposed over its scalar, vectorial and tensorial parts. The potential becomes then [8] :

$$U(\mathbf{r},\omega) = -\frac{I(\mathbf{r})}{2\varepsilon_0 c}\left[\mathrm{Re}(\alpha_s(\omega)) + (\vec{u}\times\vec{u}^*)\cdot\vec{e_z}\frac{m_J}{2J}\mathrm{Re}(\alpha_v(\omega)) + \frac{3m_J^2 - J(J+1)}{J(2J-1)}\frac{3(\vec{u}\cdot\vec{e_z})^2 - 1}{2}\mathrm{Re}(\alpha_t(\omega))\right] \tag{3}$$

where $\vec{u}$ is the polarization vector of light and $\vec{e_z}$ is the quantization axis. Hence $(\vec{u}\times\vec{u}^*)\cdot\vec{e_z}$ is the cosinus of the angle between the propagation axis and the quantization axis and $(\vec{u}\cdot\vec{e_z})$ the cosinus of the angle between the polarization axis and the quantization axis.

Furthermore, the scalar, vectorial and tensorial parts of the polarizability can be calculated from spectroscopic data with energy and lifetime of each transitions thanks to the equations of [9] (see Appendix).

Firstly, since 532nm laser are easily accessible with high power and have already been used to trap Dysprosium, we chose to work with this wavelength. However, as visible in Figure 3, there is a transition near 532nm which can create issues : a small change of the wavelength can result in a large variation of the polarizability. The position of the resonance is also not perfectly known and hence it is difficult to have a precise prediction for the value of the polarizability.

It is then clearly visible that the trapping will depend a lot on the polarization of the light and the angle of the magnetic field defining the quantization axis as shown in Figure 3.

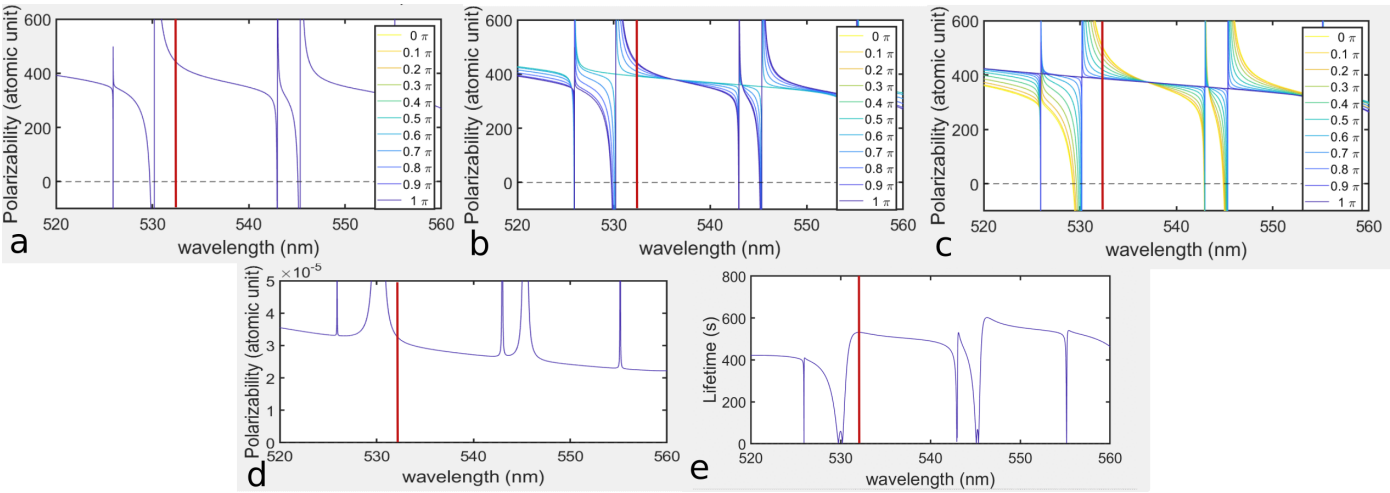


FIGURE 3 – (**a**,**b**,**c**) Real part of the polarizability of Dysprosium. The light propagates in the z direction and the magnetic field being in the (x,z) plane, the different curves are labeled by the angle of this field with the z axis. (**a**) The polarization of light is along the y axis and so always orthogonal to the field. Hence the polarizability does not depend on the direction of the field. The red line is at 532nm. (**b**) The polarization of light is along the x axis. The symmetry around $\frac{\pi}{2}$ is clearly visible. (**c**) The light is $\sigma_+$ polarized, the graph for $\sigma_-$ is the same but by changing the angle $\theta \to \pi - \theta$. For a magnetic field in the $-z$ direction, the resonances at 530nm and 545nm disappear since they are $J \to J-1$ and so the light must have $+\hbar$ angular momentum to do the transition $m_J = -8 \to -7$. (**d**) Imaginary part of the polarizability for a polarization of light along the y direction. (**e**) Lifetime of the atoms if it is limited by light scattering. At 532nm for a uniform potential of depth 100nK$\times k_B$, it is of 530s.

The first noticeable point, is the fact that the polarizabilty doesn't depends on the angle of the magnetic field if the light is linearly polarized and orthogonal to the magnetic field plane. Indeed, in that case, after any rotation in that plane, the field will stay parallel to the polarization of light. This is then the best choice for our light otherwise some small perturbations of direction of the field could change a lot the trap depth. For example with x polarization, at 532nm, we see on Figure 3 (b) that the polarizability can vary roughly between 400 a.u. and 450 a.u., and thus of 12.5%, as we rotate the magnetic field. These values seem consistent with the measured polarizability $\mathrm{Re}\,(\alpha) \in [64, 386]$ a.u.[10]

Furthermore, like for the potential, the scattering rate of the atoms depends on the scalar, vectorial and tensorial part of the polarizability :

$$\Gamma = \frac{I}{\hbar\varepsilon_0 c}\left[\mathrm{Im}\,(\alpha_s) + \mathcal{A}\cos\theta_k \frac{m_J}{2J}\mathrm{Im}\,(\alpha_v) + \frac{3m_J^2 - J(J+1)}{J(2J-1)}\frac{3\cos^2\theta_p - 1}{2}\mathrm{Im}\,(\alpha_t)\right] \tag{4}$$

And so for a given trap depth, the lifetime of the atoms can be expressed as $\tau = \frac{\hbar}{2U}\frac{|\mathrm{Re}(\alpha)|}{\mathrm{Im}(\alpha)}$. Thus to trap the atoms, the best is to have large real polarizability and small imaginary part.

At 532nm the the calculated polarizability has a real part of 450 a.u. and imaginary part of $3\times10^{-5}$ a.u. Hence for a trap depth of 100nK$\times k_B$, corresponding to an intensity of $3\times10^{-25}$ W/m$^2$ and a laser power of $3\times10^{-33}$ W, the lifetime of the atoms is of around 500s if it is limited by the light scattering. However having red detuned light, that is to say positive real polarizability, has one disadvantage : the atoms are trapped at the maximum of intensity and it is much harder to realize flat potential, whereas for blue detuned trap (negative real polarizability) it can be done easily with a black region surrounded by bright walls. There is also a possibility to do a blue detuned trap between 600nm and 700nm in the blue detuned side of a narrow transition as detailled in the Appendix. A promising regime for linear polarized light around 657nm was found with a lifetime of 144s but this will require the acquisition of a new laser source. That's why in the following, we will only focus on the red detuned trap at 532nm.

### 1.3 Tailoring the beam intensity distribution

We want to be able to generate any kind of potential for our atoms, and so we need to modulate the intensity profile of the usual gaussian laser beam. This is done using a Digital Micromirror Devide (DMD) (Vialux V-9001) controlled with a Python API wrapper [11]. It is an array of 2560x1600 individual $d = 7.6$µm wide mirrors that can be flipped by $\theta = 12°$ along their diagonal axis to reflect light in different directions. These mirrors can be in two different positions which we will call ON and OFF, depending if they reflect the light in the optical path of the setup, or not (see Figure 4). Furthermore, due to the small size of the mirror and their periodic arrangement, the DMD acts as a diffraction grating. So light, of wavelength $\lambda$, is reflected only in given directions fulfilling the constructive interference condition (see Figure 4 for the definition of the angles) :

$$m\lambda = d\,(\sin\alpha + \sin\beta) \qquad m \in \mathbb{Z} \tag{5}$$

Furthermore, the envelope of light is also reflected by individual mirrors and so we have a maximum of intensity when the reflection condition on the mirrors is also satisfied :

$$\beta = -\alpha + 2\theta \tag{6}$$

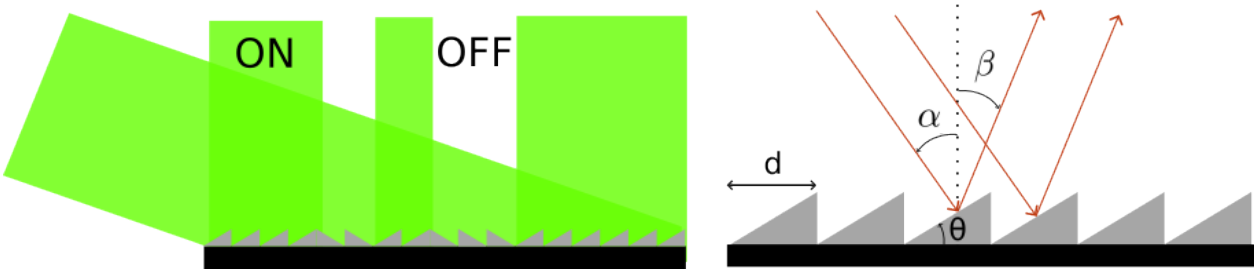


FIGURE 4 – Illustration of the behavior of the DMD with incident light. Light is visible in the directions where the rays reflected by neighboring mirrors interfere constructively.

Since we want to image as good as possible the DMD on the atomic plane to precisely shape our potential, all the DMD should be in the focal plane of the imaging setup and hence, the light must be reflected perpendicular to the DMD even if we loose a little bit of power : $\beta = 0$ is chosen. In this setting, (6) gives the maximum of intensity for $\alpha = 24°$ but this doesn't satisfy the diffraction condition (5). With our wavelength and the spacing of the mirrors the closest we can get to 24° is for $m = 6$ : The beam must illuminate the DMD with an angle of $\alpha = \text{Arcsin}\left(\frac{6\lambda}{d}\right) = 24.8°$ to be as close to the maximum of intensity as possible and have a lot of power to trap the atoms.

Following only geometrical optics, since the mirrors have only two possible states, ON and OFF, it should be possible to only generate binarized images and thus no potentials with intensity gradients. But for once, we are saved by diffraction : the beam being cut by the finite size of the optics, a point of the object is not imaged as a point but as a point spread function, which is well approximated, for spherical optics, by an Airy disk [12] :

$$I(r) = I_0 \left( \frac{J_1\left(\frac{\pi r}{a}\right)}{\frac{\pi r}{a}} \right)^2 \tag{7}$$

where $J_1$ is the Bessel function of the first kind of first order.

This intensity vanishes for the first time at a radius of $1.22 \times a$ : that defines the resolution of the setup. So to be distinguishables, two neighboring objects must have their images separated by more than this distance. Thus in our case, if two neighboring mirrors are not distinguishable, we can group them as patches of mirrors that behaves, in the image plane, as if they where only one point. Thus depending on the number of mirrors we turn ON in this patch, the quantity of reflected light will change and so different intensities can be reached. Some simulated examples with patches of 5x5 mirrors are shown in Figure 5.

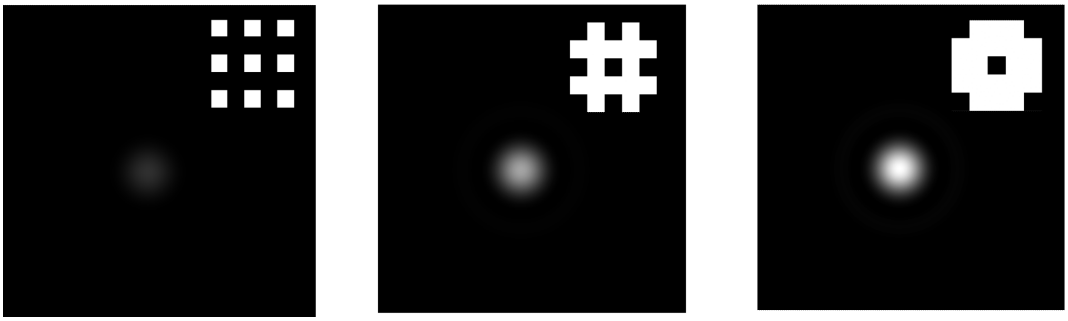

FIGURE 5 – Example of the variation of the observed intensity when the number of ON mirrors changes. The simulations are made with a Airy disk with resolution of 0.6µm corresponding to patches of 5x5 indistinguishables mirrors. On the top right corner are shown the mirror pattern displayed, from left to right there are 9,16 and 20 mirrors turned ON.

The first possibility to grayscale our image is then to divide it in patches of indistinguishables mirrors and display on each of these patches the appropriate number of mirrors to have the wanted grayscale : this is Bayer dithering [13]. However, this divisions into patches creates some artifacts in the binarized picture mostly in the form of straight lines appearing in the uniform regions as visible in the sky of Figure 6 (a).
Therefore, we will instead use error-diffusion dithering with the Floyd-Steinberg algorithm [14]. It works as follows for pictures with intensity between 0 and 1 : The value of the top left pixel is rounded to 0 if its value is below 0.5 and to 1 otherwise. Then the difference between this rounded value and the true one is calculated and redistributed to the neighboring pixels with the weights defined by the kernel :

$$\begin{bmatrix} 0 & * & \frac{7}{16} \\ \frac{3}{16} & \frac{5}{16} & \frac{1}{16} \end{bmatrix}$$

The rounded pixel is represented by $*$ and the values are chosen such that an uniform intensity of 0.5 will result in a checkerboard pattern.

Then the picture is scanned from left to right and top to bottom. Furthermore, no error is redistributed to already rounded pixels, as visible in the redistribution kernel : this allows to only scan the picture once.

This results in a much better dithering, without the artifacts but only some apparent noise in the large uniform areas, as shown in Figure 6 (b).

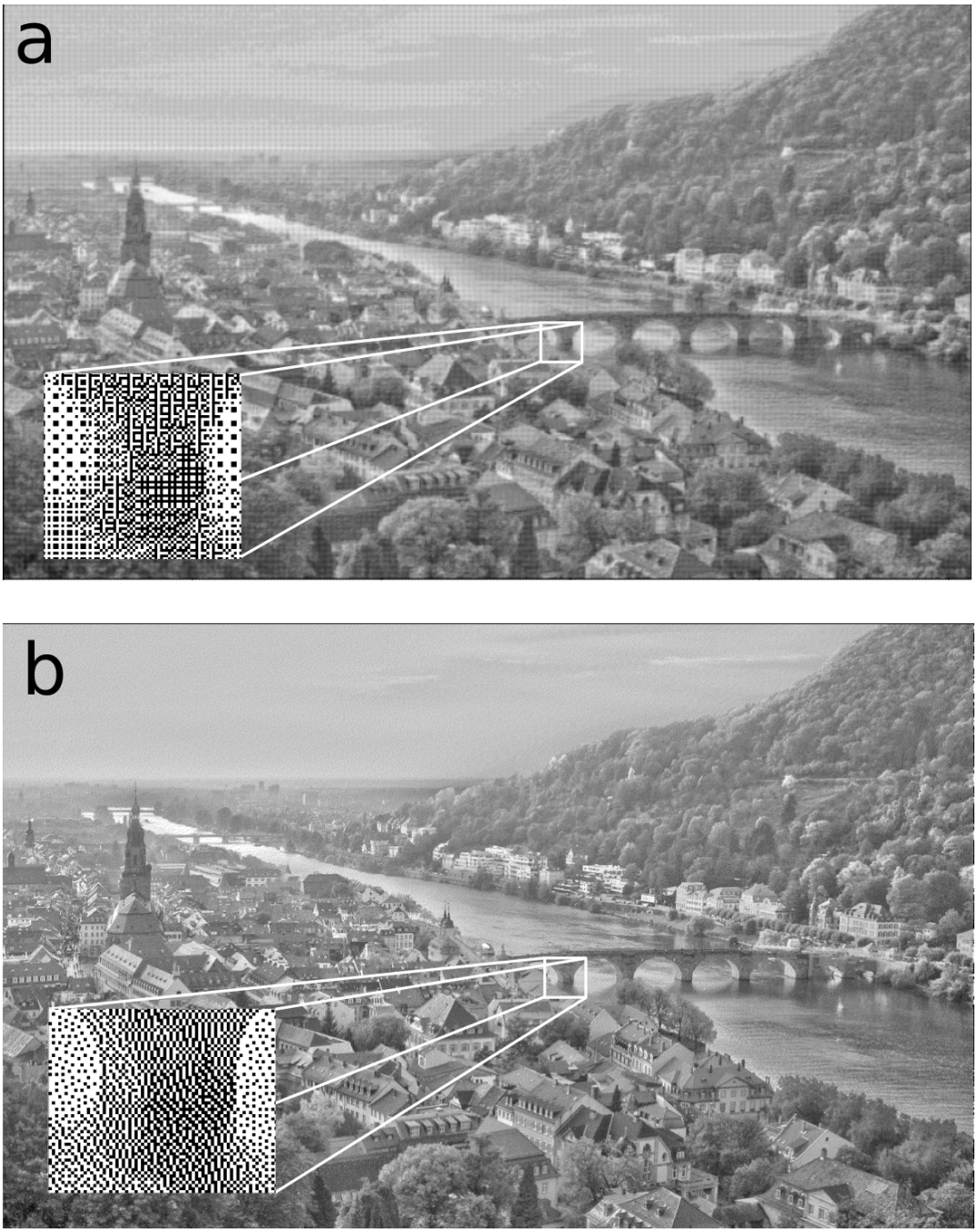


FIGURE 6 – (**a**) Bayer dithering for patches of 5x5 mirrors, some straight lines artifacts appear in the sky for example. On the zoomed part, individual patches are visible. (**b**) Floyd-Steinberg dithering, the defects due to dithering seem less important. Individual mirrors are visible in the zoomed part.

# 2 Experimental realisation

This part will explain how we will generate a tailored intensity distribution in a test setup to later trap Dysprosium atoms.

## 2.1 Experimental setup

We will first describe the test setup used throughout the internship to create these tailored traps. We need to first illuminate the DMD screen and then image it on the horizontal plane where the atoms are supposed to be. The atoms are not here and hence replaced by a microscope objective (7 in Figure 7) and a camera imaging the assumed position of the atoms.

First of all, to be able to generate the largest variety of traps, we need to be able to use all the mirrors of the DMD and to have an image in the atomic plane not larger than the field of view of the objective used to image the DMD on the atoms. So the incident beam on the DMD must be collimated and have a beam diameter as large as the short axis of the DMD, but not more to avoid stray light reflected by the mount of the DMD. We estimate that we need a beam waist of 6mm. We use fiber coupled light with oucoupler of focal 25mm and fiber of numerical aperture 0.07 leading to a beam waist of 1.75mm. Thus a telescope (2 in Figure 7) is formed by a $f_0 = -60$mm and a $f_0' = 200$mm lenses having hence a magnification of 3.3, to enlarge the beam. The incident beam on the DMD has then a measured beam waist of 5.2mm. Second, the imaging objective having a field of view of 150µm, a demagnification of around 80 must be done during the imaging on the atomic plane. This is achieved with two 4f-setups, a first one with lenses of focals $f_1 = 250.9$mm and $f_1' = 50$mm resulting in a demagnification of 5.02 and a second one with a lens of $f_2 = 501.8$mm and the Special Optics objective of effective focal length $f_2' = 32.2$mm achieving a demagnification of 15.58 giving to the final setup a demagnification of 78. However, since the Special Optics objective cannot be used for the test setup, the second telescope is made with a lens of focal 125mm and a Mitutoyo objective of focal 10mm and thus the demagnification is of only 63. In both cases, the final objective is placed on a 5 axis translation stage. The test setup is depicted in Figure 7 while the setup that will be implemented in the main experiment is presented in Appendix.

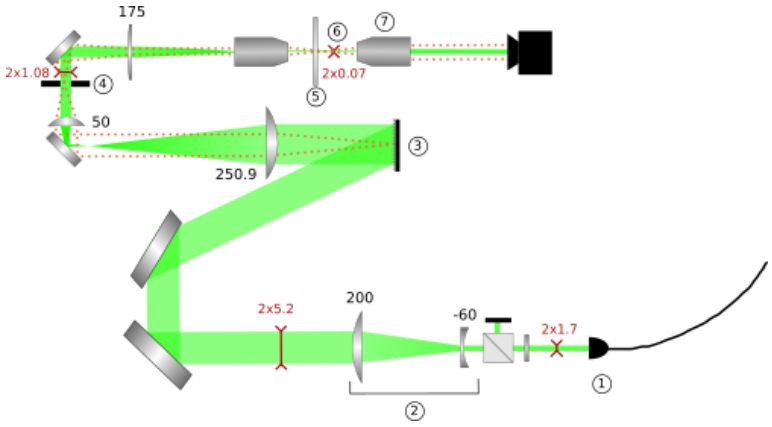


FIGURE 7 – Description of the experimental setup. All the distances are in mm. The red arrows are twice the beam waist. The beam exit the fiber outcoupler (1) with a beam waist of 1.7mm and then its polarization is cleaned. It is enlarged by the telescope (2), before being reflected by the DMD (3) and passing by two telescopes such that the beam waist in the fictional atomic plane (6) is of 70µm. The image is then magnified by 7 with a microscope objective (7) to be observable on a camera. Between the two telescopes, at the position of the intermediate image, an iris (4) is placed to remove the high diffraction orders of the DMD and reduce the resolution of the setup. The green rectangles represent the beam, which is collimated between each 4f-setup, and the orange dashed lines are two light rays coming from the DMD : the image is at infinity inside each telescope and projected on the atomic plane.

To simulate as well as possible the final setup in the test one, a viewport (5), identical to the one on the main experiment, is added just before the fictional atomic plane. Furthermore, since the image of the DMD is too small to be directly imaged, a microscope objective is added to enlarge it by 7 before projecting the image on the camera.

To be able to grayscale the image, we first need to ensure the resolution of the setup is not too good, so that the images of neighbouring mirrors overlap each other. An iris is inserted at the position of the intermediate image of the DMD formed by the first 4-f setup and we measure the resolution for different opening of the iris. Patches of 5x5 mirrors are displayed successively over the DMD and the intensity is fitted by an Airy disk (7). The resolution being then $1.22 \times a$.

A first measurement is made with the iris fully open (Figure 8 (b)) and we obtained, on average over the DMD screen, a resolution of $1.8 \pm 0.2$µm. However, the microscope 7 (see Figure 7) used for imaging in the test setup has a numerical aperture of 0.25 giving a theoretical resolution of $d = \frac{1.22\lambda}{2NA} = 1.3$µm. The measured resolution being close to this value, this objective might be the limiting factor and the real resolution on the atomic plane be of only 0.6µm as simulated with Zemax Optic Studio (Figure 8 (a)). The diagonal of the image of a mirror being $\sqrt{2} \times 7.6/63\ \mu$m $= 0.17$µm, the point spread function covers only patches of 3x3 mirrors, not enough to grayscale well the image.

Therefore, the iris is closed as much as possible and a new measurement is made (Figure 8 (c)) leading to a resolution of $2.2 \pm 0.2$µm. This clear decrease of the resolution shows that the iris is now the limiting factor, and hence this is also the resolution on the atomic plane. This leads to patches of 12x12 mirrors for the grayscales in the test setup and of 15x15 in the final one.

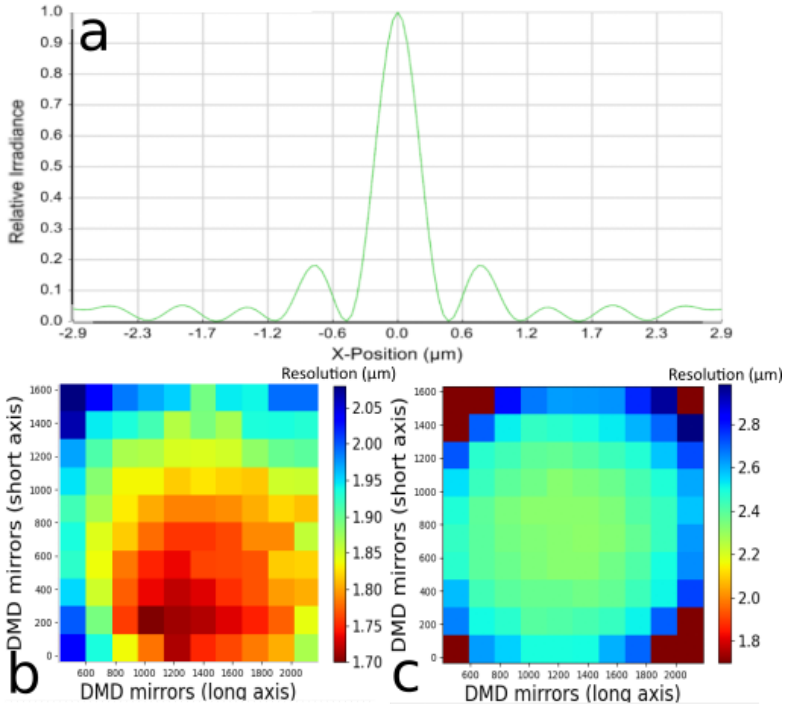


FIGURE 8 – (**a**) Theoretical Point Spread Function of the final setup on the atomic plane simulated with Zemax, the value of the resolution is the first zero, that is to say a little less than 0.6µm. (**b,c**) Resolution for point at different positions over the DMD, with iris open (b), or close (c). The variations over the DMD are due to non perfect alignment as well as geometrical aberrations. Finally, there are some unreliable values in the corners because here the intensity of the incoming gaussian beam is too small and so there are not enough illuminated pixels on the camera to fit the image properly.

## 2.2 Optimization of the trap

It is now time to shape our potential, and we start by trying to generate a flat top beam ; this is done using the following algorithm (inspired by [15]) presented in Figure 9 :

1) A small patch of 5x5 mirror is displayed at the center of the DMD to locate its position on the camera.

2) Two of these patches, separated by 400 mirrors, are displayed . Their separation on the image allows to calculate the demagnification on the camera.

3) All the mirrors of the DMD are turned ON (this define the background pattern of the mirrors) to get an image of the incident beam and the RMS contrast (standard deviation) of the intensity is calculated.

4) Using the measured position of the center and demagnification as well as the 45° angle of the DMD with the camera axis, a rotation and rescaling of the image is made to associate each mirror to the group of pixels of the camera where its image is projected.

5) The image goes into a low pass filter with cut-off frequency of $f_c = 10^4$ m$^{-1}$ on the atomic plane to start by correcting only the low frequency defects. This frequency is approximately the one of the size of the image.

6) Since the intensity is the square of the field, the inverse of the square root of the image is calculated, multiplied by the background pattern, then grayscaled using the Floyd-Steinberg algorithm to be displayed on the DMD. The reflected field should then be at n$^{\text{th}}$ iteration $E_n = \frac{E_{n-1}(x,y)}{\sqrt{I_{n-1}(x,y)}}$ and thus close to uniform.

7) A new image is taken and the RMS contrast is calculated : if it is smaller than the previous one, the pattern is accepted and becomes the new background pattern, otherwise the cut-off frequency is multiplied by 2 : $f_c' = 2 \times f_c$ to start to correct smaller defects

8) We go back to step 4)

A total of 20 iterations of this loop are made, since no clear improvement were visible most of the time after the 15$^{\text{th}}$ one.

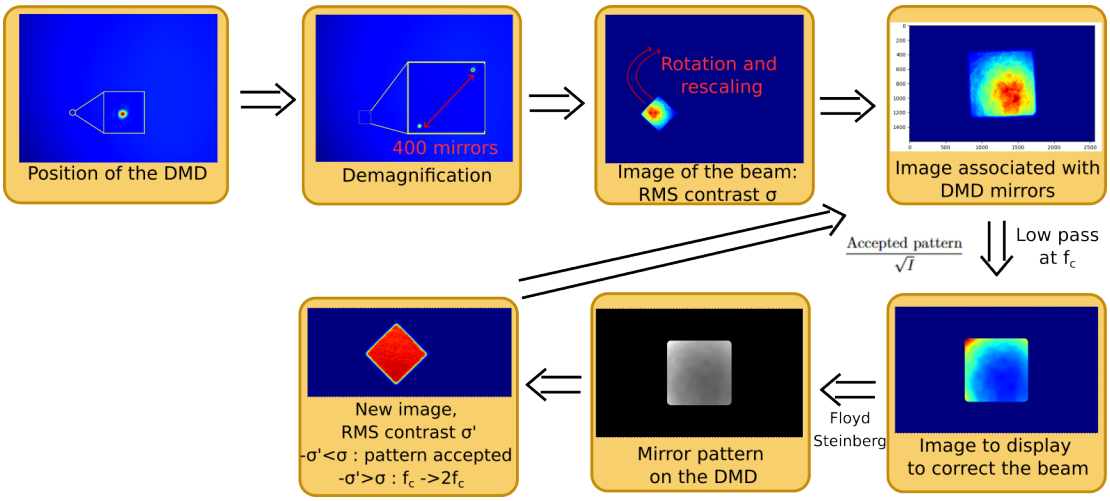


FIGURE 9 – Description of the optimization algorithm (see text), after 10 to 15 iterations of the depicted loop, it no longer manages to improve the flatness of the intensity.

We observed that, trying to reach a perfect flat top, with intensity of 1 in a given region and 0 outside leads to oscillations of the intensity in the border region as seen in Figure 10 (a). Indeed, since the iris is almost closed, the high frequencies of the image are filtered out while they are necessary to generate abrupt variations : this is the Gibbs phenomenon in Fourier analysis [16]. Therefore, the targeted image is changed to be a flat top with smooth borders of intensity $I = \frac{I_0}{1+\left(\frac{r}{r_0}\right)^{\alpha}}$, where $I_0$ is the intensity of the flat top, $r$ the distance, in mirrors, from the border and $(\alpha, r_0)$ two tunable parameters.

To find the best values for these parameters, the mean RMS contrast, reached after three distinct runs of the optimizations algorithm, is measured for different values of $r_0$ and $\alpha$. The results are presented in Figure 10 (b). The best RMS contrast is obtained for $\alpha = 6$ and $r_0 = 50$ and hence these values are chosen for the border section. Luckily, these smooth borders are not just better for having a flat top, but it has also been shown theoretically [17] that soft-walled potential are better to have homogeneous dipolar quantum gases.

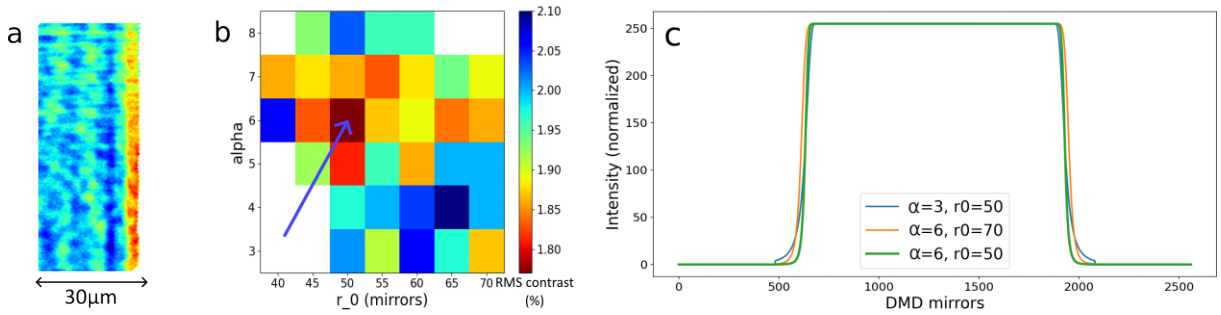


FIGURE 10 – (**a**) Observation of the oscillations of the intensity near a sharp wall. (**b**) RMS contrast of the picture after the optimization process for different values of the parameters $\alpha$ and $r_0$, even if the distribution seems a little bit random, small $\alpha$ give worse results as well as too large $r_0$, while the region around (6,50) is on average better. (**c**) Cut of the target flat top for different $(\alpha, r_0)$. The blue curve has a discontinuity when we reach the borders of the DMD. The thick green line is the one chosen.

With these improvements and an alignment of the setup as good as possible, flat top squares 120µm wide in the atomic plane with RMS contrast below 1.3% are reached, with an example shown on Figure 11 (a) with a cut on Figure 11 (b).

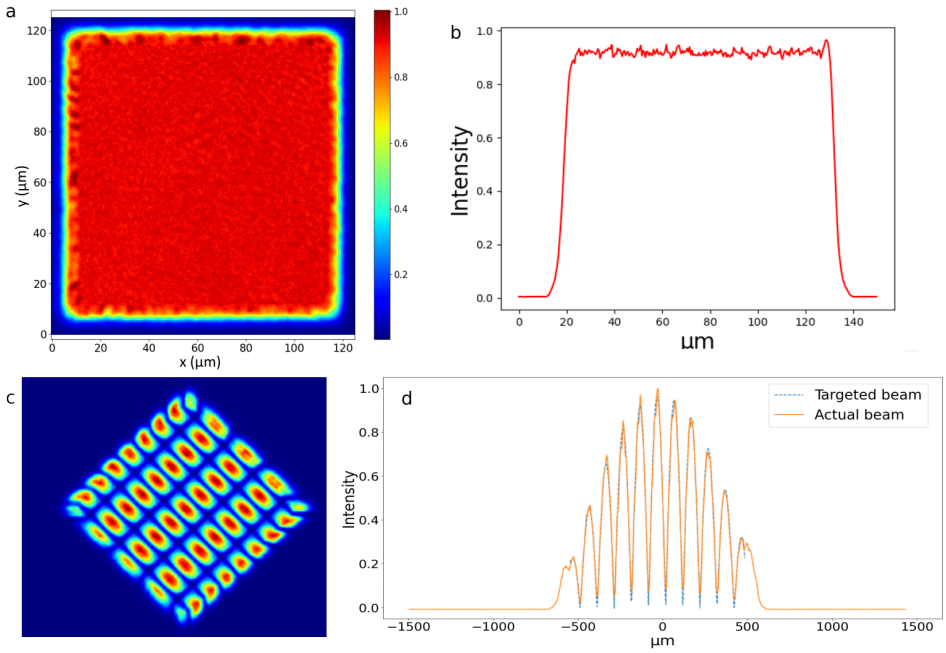


FIGURE 11 – (**a**) Example of Flat top obtained after the optimization process, here the RMS contrast is of 1.27%. In (**b**) a cut of the intensity is shown.(**c,d**) show the image and cut of a beam with targeted intensity $I(X,Y) = I_0 \sin(f_x X) \sin(f_y Y)$.

Furthermore, it is also possible to generate more complicated potentials : indeed, in the optimization algorithm, if we calculate the standard deviation around the targeted intensity $I_t(x, y)$ and multiply, in step 6, $E_n$ by the square root $\sqrt{I_t(x, y)}$, the algorithm will converge no longer to a flat top but toward the desired potential. One example of lattice potential is shown in Figure 11 (c,d). However, unlike the flat top case where we can directly calculate the standard deviation, here, it must be calculated around the value of the targeted beam and so, the picture and the target must have the same normalization. To ensure this point, they are normalized such that the two have the same mean ; indeed, since the picture has a lot of fluctuations, if the normalization is made with respect to the maximum, noise of the measured intensity of this pixel can change a lot the result, while the mean has the advantage to be not influenced by these fluctuations because their mean value is 0 (Figure 11 (d)).

## 2.3 Stability of the trap

Once a tailored intensity profile has been created, it is important to ensure the stability of the potential over time. Three main effects need to be taken into account :

First, the power of the laser source must be very stable to not change the depth of the potential, this is not the case in this test setup, but in the final setup the power will be stabilized using AOM.

Next, the setup must be mechanically stable such that the position of the image doesn't move over time.

Finally, perturbations in the environment like for example variation of the temperature of the lab, can change the optical index of air and hence disturb the picture.

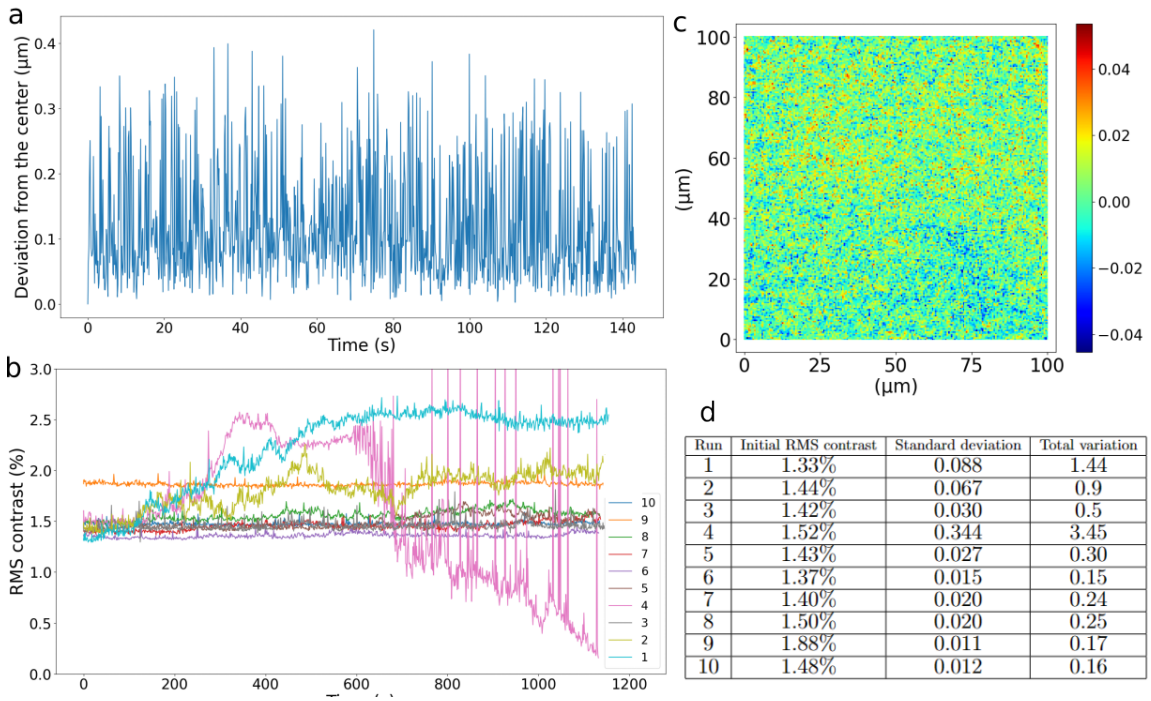


| Run | Initial RMS contrast | Standard deviation | Total variation |
|---|---|---|---|
| 1 | 1.33% | 0.088 | 1.44 |
| 2 | 1.44% | 0.067 | 0.9 |
| 3 | 1.42% | 0.030 | 0.5 |
| 4 | 1.52% | 0.344 | 3.45 |
| 5 | 1.43% | 0.027 | 0.30 |
| 6 | 1.37% | 0.015 | 0.15 |
| 7 | 1.40% | 0.020 | 0.24 |
| 8 | 1.50% | 0.020 | 0.25 |
| 9 | 1.88% | 0.011 | 0.17 |
| 10 | 1.48% | 0.012 | 0.16 |

FIGURE 12 – (**a**) Deviation of the position of the center of the DMD on the camera over time. Its position is calculated by displaying a 5x5 mirrors patch on the center of the DMD and fitting the image by an Airy disk. (**b**) Evolution of the measured RMS contrast over time for 10 different flat top pattern displayed on the DMD. The standard deviation of this RMS contrast as well as the difference between the maximum and minimum values reached are presented in table (**d**). (**c**) Difference between the final and initial image of the trap for the run 10 of (**b**). The two pictures where renormalized such that their mean intensity is 1, so the variations observed are of the order of 4% of the intensity and seem distributed randomly.

Apart from having very well screwed optical elements, it is necessary to isolate as much as possible the DMD from its control board to have mechanical stability. Indeed, the control board is active cooled and this fan induces vibrations in the board that are transmitted to the DMD via the ribbon cables between them. To do so, some foam is pressed on these cables to dampen the oscillations as suggested in [18]. The stability is then tested by following the position of the center overtime. As shown in Figure 12 (a), over more than 2min, the center moves less than 0.4µm : this is 0.3% of the size of the trap and 18% of the resolution size of the setup. The position can be considered stable !

To test now the stability of the trap, the optimization algorithm is run until a good flat top is reached, then the obtained pattern is displayed for 20min during which an image is taken every second and the RMS contrast is calculated ; this process is then repeated 10 times over one night. The results are summarized on Figure 12. Not taking into account some unstable curves, the standard deviation of the flatness of the images is on average of 2% of the initial value and hence the trap is sufficiently stable to consider that the trap is the same in successive shots, ensuring the reproducibility of the experiment. However, there are some interesting facts to highlight : First of all the $4^{\text{th}}$ curve seems surprising, after 600s the RMS contrast decreases and thus the flatness improves but in a very noisy way. In fact, looking at the pictures at the end, one sees that they are completely saturated, probably due to fluctuations of the power of the laser diode. This creates then a false impression of flatness of the intensity and confirm the importance of power stability. Furthermore, the first two runs are way less stable and it can be explained quite easily. These datas were taken at the end of the day when there were still activities in the lab, and so small perturbations of the environment, while the others happened during the night. It indeed shows the importance of isolating as much as possible the setup from the environment which will be much better in the final experimental setup. Finally, it has not been possible to test the stability of the trap on timescales shorter than the second. Indeed the time needed to take a picture and extract the RMS contrast is of the order of one second. So unfortunately we cannot test how stable the trap is during the illumination time planned during one run of the experimental sequence, which is of the order of 100ms.

# 3 Simulation of the condensate

We realized flat top traps with RMS contrast below 1.5% but one remaining question is how flat should be the potential such that the perturbations are not felt by the BEC ? This part will try to answer this question by simulating the ground state of the BEC in the obtained trap.

## 3.1 Theoretical background

First of all, our atoms of Dysprosium are confined by the harmonic accordion lattice in a quasi-2D regime. We can thus separate the wave function over the $z$ component and the in plane wave function $\Psi\left(\overrightarrow{\rho},z\right)=\psi\left(\overrightarrow{\rho}\right)\phi\left(z\right)$, where $\phi\left(z\right)=\left(\pi l_z^2\right)^{-1/4}e^{-\frac{z^2}{2l_z^2}}$ is the ground state of the harmonic oscillator in the z direction and $l_z=\sqrt{\frac{\hbar}{m\omega_z}}$ is the confinement length in the $z$ direction : here for trapping frequency of 5 kHz, we have $l_z=0.11$ µm.

Injecting this wavefunction into the Gross Pitaevskii equation (2) and integrating over the $z$ direction, one get the effective 2D equation [19] :

$$i\hbar\frac{\partial\psi}{\partial t}=\left[-\frac{\hbar^2}{2m}\nabla_\rho^2+V\left(\overrightarrow{\rho}\right)+\frac{4\pi\hbar^2a_s}{\sqrt{2\pi}ml_z}|\psi|^2+\Phi_{dd}\right]\psi \tag{8}$$

where the dipolar interaction term is the convolution :

$$\Phi_{dd}\left(\overrightarrow{\rho}\right)=\int U_{dd}^{2D}\left(\overrightarrow{\rho}-\overrightarrow{\rho}'\right)|\psi\left(\overrightarrow{\rho}'\right)|\mathrm{d}\overrightarrow{\rho}' \tag{9}$$

The Fourier transform of the 2D effective dipolar interaction can be expressed analytically as a function of the angle $\alpha$ of the dipoles with the $z$ direction [19] :

$$\mathcal{F}\left(U_{dd}^{2D}\right)\left(\overrightarrow{k}\right)=\frac{\mu_0\mu_m^2}{3\sqrt{2\pi}l_z}\left[F_\parallel\left(\overrightarrow{q}\right)\sin^2\alpha+F_\perp\left(\overrightarrow{q}\right)\cos^2\alpha\right]\qquad\text{with}\,\overrightarrow{q}=\frac{l_z}{\sqrt{2}}\overrightarrow{k} \tag{10}$$

And if we define the $x$ axis such that the dipoles are in the ($x$,$z$) plane, $F_\parallel$ and $F_\perp$ have the following expressions :

$$\begin{cases} F_\parallel\left(\overrightarrow{q}\right) &= -1+3\sqrt{\pi}\frac{q_x^2}{q}e^{q^2}\mathrm{erfc}\left(q\right)\\ F_\perp\left(\overrightarrow{q}\right) &= 2-3\sqrt{\pi}qe^{q^2}\mathrm{erfc}\left(q\right)\end{cases} \tag{11}$$

where $q$ is the norm of the $q$ vector and erfc the complementary error function $\mathrm{erfc}\left(x\right)=\frac{2}{\sqrt{\pi}}\int_z^\infty e^{-t^2}\mathrm{d}t$.

Let's look now at our specific case of flat top potential. In the case of a uniform potential, the solution for the condensate is a uniform density except in a region close to the border where the density decreases to zero. The size of this region is given by the healing length. Assuming the healing length is much smaller than the system size, we will here neglect these variations. To describe the effect of potential imperfections, we consider a uniform potential $V_0$ with some small perturbation $\delta V$ of zero mean such that the total potential is : $V=V_0+\delta V$. We finally treat the ground state via first order perturbation and assume that its wavefunction can be written : $\psi=\sqrt{n_0l_z}+\psi^{(1)}$ where $n_0=\frac{N}{\sqrt{\pi}l_z\times L^2}$ is the 3D density of atoms in the trap.

Furthermore, since we search a time independent density, we will look only at the spatial variations and replace in equation (8) $i\hbar\frac{\partial\psi}{\partial t}$ by $\mu\psi$, where $\mu$ is the chemical potential [2].

At order 0 in perturbations, one get the chemical potential (the conservation of the number of atoms in the perturbation ensures that this potential stay the same at first order (see Appendix)) :

$$\mu=\frac{4\pi\hbar^2a_s}{\sqrt{2\pi}m}n_0\left[1+\varepsilon_{dd}\left(3\cos^2\alpha-1\right)\right] \tag{12}$$

with $\varepsilon_{dd} = \frac{m\mu_0\mu_m^2}{12\pi a_s \hbar^2}$ the ratio of the strength of dipolar and contact interactions.

This chemical potential allows us to calculate the healing length of our system $l_h = \sqrt{\frac{\hbar^2}{m\mu}}$. This is the length scale over which the density varies at the borders of the trap. For a density of $10^{21}$ atoms/m$^3$, which is the one used in all the following, dipoles aligned in the $z$ direction, and scattering length of $a_s = 110a_0$ the healing length is of the order of 0.1 µm and so 0.1% of the typical size of our trap. Furthermore, since $\mu$ scales with $\sqrt{n_0}$, this conclusion stay true for a wide range of density. Thus it was reasonable to assume a uniform density and neglect the effects of the borders.

For the expansion at first order, we will decompose the perturbations over their Fourier components $\delta V\left(\overrightarrow{\rho}\right) = \int \delta V_{\overrightarrow{k}} e^{i\overrightarrow{k}\cdot\overrightarrow{\rho}} \mathrm{d}\overrightarrow{k}$ and $\psi^{(1)}\left(\overrightarrow{\rho}\right) = \int \psi_{\overrightarrow{k}} e^{i\overrightarrow{k}\cdot\overrightarrow{\rho}} \mathrm{d}\overrightarrow{k}$. One can then calculate the density perturbation as a function of the potential perturbations :

$$\psi_k = \frac{-\sqrt{n_0 l_z}}{\frac{\hbar^2 k^2}{2m} + 2 \times \frac{4\pi\hbar^2 a_s}{m\sqrt{2\pi}} n_0 \left[1 + \varepsilon_{dd}\left(3\cos^2\alpha - 1 + 3\sqrt{\pi}\frac{q_x^2}{q} e^{q^2}\mathrm{erfc}\left(q\right) - 3\sqrt{\pi} e^{q^2}\mathrm{erfc}\left(q\right)\left(\frac{q_x^2}{q} + q\right)\cos^2\alpha\right)\right]} \delta V_k \tag{13}$$

And from this formula, one can directly compute at first order the density of atoms :

$$n_{2D} = \left|\sqrt{n_0 l_z} + \psi^{(1)}\right|^2 = n_0 l_z + 2\sqrt{n_0 l_z}\mathrm{Re}\left(\psi^{(1)}\right) \tag{14}$$

We see that $n_{2D}$ is a function mainly of the mean 2D atomic density $n_0 l_z$, the s-wave scattering length $a_s$ and the ratio of dipolar and contact interactions $\varepsilon_{dd}$. In contrast to the purely contact case, where the equation (13) is a Lorentzian with main component at $k = 0$, here the interaction term is a function of $q$ and then the main contribution can be at a non zero wavevector : this is a consequence of the long range effects of the dipolar interactions. Furthermore, the fact that $\psi_k$ is a function of $q_x$ shows the anisotropic dipolar interactions and thus this can create anistropic perturbations. However, in the case of all dipoles pointing in the $z$ direction, that is to say $\alpha = 0$, the $q_x$ cancels out, and we recover isotropic perturbations. Finally, one interesting fact, is that the dipolar interactions can induce mean-field instabilities. Indeed if we look for example at low frequency perturbations $k \to 0$, the denominator becomes $2 \times \frac{4\pi\hbar^2 a_s}{m\sqrt{2\pi}} n_0 \left[1 + \varepsilon_{dd}\left(3\cos^2\alpha - 1\right)\right]$ and this can vanish for a given $\alpha$ if $\varepsilon_{dd} > 1$, that is to say larger dipolar interactions than contact ones. This is a well known fact of ground state calculations [1], which luckily appears also in this potential perturbation calculations. However, in that case one Fourier mode of the density perturbation will diverge and we will no longer be in the small perturbation regime used in the derivation. In reality there would be stabilisation of exotic states as supersolids, but this need more complex theory to treat it beyond the scope of the present work (see [1]).

## 3.2 Numerical results

In all this subsection, we will consider the atoms in a trap of mean depth $U_0 = k_b \times 100\mathrm{nK}$ while the values of the s-wave scattering length $a_s$, the atomic density $n_0$ and the ratio of contact and dipolar interactions $\varepsilon_{dd}$ will vary.

First of all, we need to find for which values of the parameters we have no instability and are in the small perturbations regime. Since the instability occurs when the denominator of (13) vanishes, its existence can be probed by a change of sign. This is summarized in Figure 13 : it represents the smallest angle $\alpha$ at which the instability occurs, with value for the trapping frequency along $z$ of $\nu_z = 5\mathrm{kHz}$ and the dipolar scattering length of Dysprosium $a_{dd} = \frac{m\mu_0\mu_m^2}{12\pi\hbar^2} = 133a_0$ where $a_0$ is the Bohr radius. We clearly see that the instability happens only when the s-wave scattering length is smaller than the dipolar one, confirming the threshold

$\varepsilon_{dd} > 1$. Furthermore, as $a_s \to a_{dd}$, the critical angle increases toward $\frac{\pi}{2}$, the dipoles need to point as much as possible in the atomic plane to maximise the dipolar interaction and be above the contact ones.

Thus to stay in the condition of validity of the small perturbations, we will always keep $\varepsilon_{dd} < 1$ or stay at small angle $\alpha$.

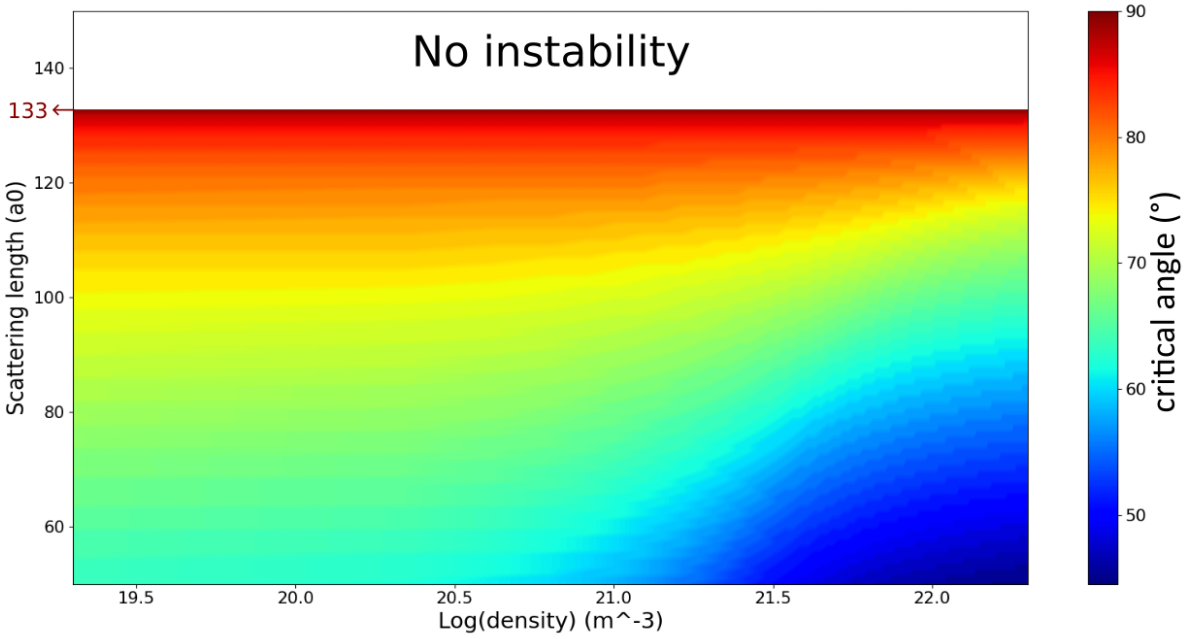


FIGURE 13 – Smallest angle of the dipoles with the vertical confinement direction, at which the instability occurs for different density and s-wave scattering length. A given set of parameters, ($n_0$,$a_s$,$\alpha$) is considered to have at least one unstable wave vector $\overrightarrow{k}$ if the denominator of (13) changes of sign. There are no instability for $a_s$ above $133a_0$ as expected. We also see that as the scattering length increases toward $133a_0$ the critical angle tends to $\frac{\pi}{2}$. Furthermore, we also see that as we increases the density, the system becomes more unstable.

We start by looking at the influence of each Fourier component, of the perturbation of the potential, on the perturbation of the density. To do so, a pure sinusoidal perturbation of the potential is created $\delta V = 2\delta V_0 \cos kr$ with $\delta V_0 = 1.5 \times 10^{-2} U_0$ and the density perturbation is computed using equation (13). The results are shown in Figure 14 for a density $n_0 = 10^{21}$ atoms/m$^3$. First of all, as expected with formula (13), the purely contact case is a Lorentzian with a value at $k = 0$ decreasing with $a_s$. Furthermore, in the dipolar case, a maximum at finite $k$ appears whose amplitude increases with $\varepsilon_{dd}$ (Figure 14 (b)) The position of this maximum seems to stay roughly the same at a constant $a_{dd}$ (Figure 14 (c)). This maximum also increases and shift to low frequencies when the dipoles are tilted (Figure 14 (d)).

The fact that the amplitude of the perturbation increases with $\varepsilon_{dd}$, is caused by the decrease of contact interactions through $a_s$ as visible in Figure 14 (b) and Figure 15 (b). Furthermore, the fact that the position of the maximum does not depends on $a_s$ but only on $a_{dd}$ (Figure 14 (c)), let think that this position is entirely set by the competition between the dipolar and kinetic parts of equation (13) and not on the contact interaction. Indeed, if we look at equation (13), the contact part is not a function of $k$ and thus changing $a_s$ only change the denominator by a constant value. This is different from the roton minimum in the dispersion relation, where the scattering length $a_s$ also play in the competition [1, 20]. Finally, the shift to low frequencies with the tilting angle of the dipoles (Figure 14 (d)) can be explained by the fact

that tilting the angle is roughly equivalent to making the dipolar interaction less repulsive as we create one attractive direction. Thus the kinetic part compensate the dipolar one at lower $k$.

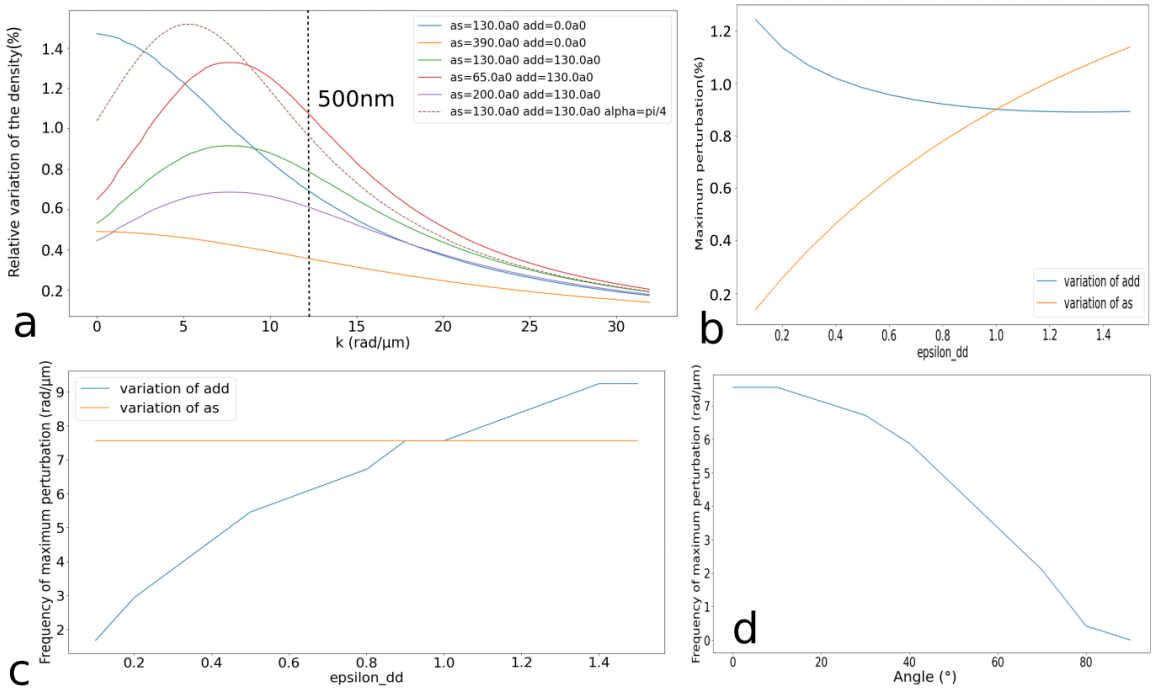


FIGURE 14 – Relative importance of each Fourier component on the perturbation of the density. All the curves are plotted with a background density $n_0 = 10^{21}$atoms/m$^3$. (**a**) Amplitude of the perturbation as a function of the wavevector for different parameters ($a_s$,$a_{dd}$). Except for the purple dotted line, all the curves are for $\alpha = 0$. The black dotted vertical lines, corresponds to defects of the size of the wavelength : smaller defects, and so higher $k$ are not expected. (**b**) Amplitude of the maximum of the curve of (**a**) as a function of $\varepsilon_{dd}$. For the orange curve $a_{dd}$ is held constant at $133a_0$ and $a_s$ varies to have the right $\varepsilon_{dd}$, while for the blue one this is the opposite ($a_s$ held constant at $133a_0$). (**c**) Position of the maximum of the curve of (**a**) as a function of $\varepsilon_{dd}$. This position changes only when $a_{dd}$ is varied. (**d**) Position of the maximum of the curve of (**a**) as a function of the angle $\alpha$. These are calculated for $a_s = 200a_0$ and $a_{dd} = 133a_0$

Let's now look at the influence of the different parameters on the perturbations of the density. First of all, it is clear from the equation (13), that the perturbation of density are linear in the perturbation of the potential, so from now, we will always consider perturbations with a standard deviation of 1.5% of $U_0$. To be as general as possible, the potential is perturbed with white noise with amplitude such that the standard deviation is the targeted one. This noise has frequencies between $k_{min} = 0.04$ rad/µm and $k_{max} = 6$ rad/µm. The maximum frequency is chosen such that it correspond to a discretization of roughly the size of the wavelength of the trapping light, which is the smallest size of defects we can hope to correct. The minimum frequency correspond to a size of 70µm that is approximately the size of the trap we will use. Then the relative variation of the density, $2\frac{\mathrm{Re}(\psi^{(1)})}{\sqrt{n_0 l_z}}$ is numerically calculated as a function of the different parameters ($n_0$,$a_s$,$\alpha$). The results are presented in Figure 15.

Firstly, it is clear in Figure 15 (a) that the variations of the density decrease as the background density $n_0$ increases : Two main regimes seems to exist : First at low densities, the relative variations scales as $n_0^{-\beta}$ with $\beta = 0.588 \pm 0.004$ while at high densities, it scales as $n_0^{-\gamma}$ with $\gamma = 0.9832 \pm 0.0007$. The two

regimes are separated around a density such that the kinetic and interactions term are of the same order : $\frac{\hbar^2 k^2}{2m} \simeq \frac{8\pi\hbar^2 a_s}{m\sqrt{2\pi}} n_0$, that is to say $n_0 = \frac{k^2}{8\sqrt{2\pi}a_s}$.Depending on the value of $k$ between $k_{min}$ and $k_{max}$ we use, we have this critical density ranging from $n_{0_{min}} = 10^{16}$ atoms/m$^3$ and $n_{0_{max}} = 3 \times 10^{20}$ atoms/m$^3$. Looking at Figure 15 (a), the transition seems to be close to $\log n_{0_{max}} = 20.4$ this mean that we enter in the high density regime, when the interaction term is larger than the kinetic one at all the frequencies that are in the noise.

Furthermore, there is also a decrease of the perturbations as the s-wave scattering length increases as visible in Figure 15 (b). However, these variations are much smaller than those induced by a change of the mean density (see Figure 15 (b,c)). Additionally, the presence of dipolar interaction reduces further the scattering length effect. In our case, the best parameter to reduce the fluctuations of the density of atoms dues to the non perfect flat top, is to work with high density of atoms.

Finally, when the angle $\alpha$ of the dipoles with the $z$ direction varies, the perturbations in the density increases (see Figure 15 (c)) and when $\varepsilon_{dd}$ is close to 1, these variations become much larger for angles near $\frac{\pi}{2}$ as we are approaching the instability. In that case, we would need more complex theory to describe the system (see [1]). There are also obviously no variations when there is only contact interactions.

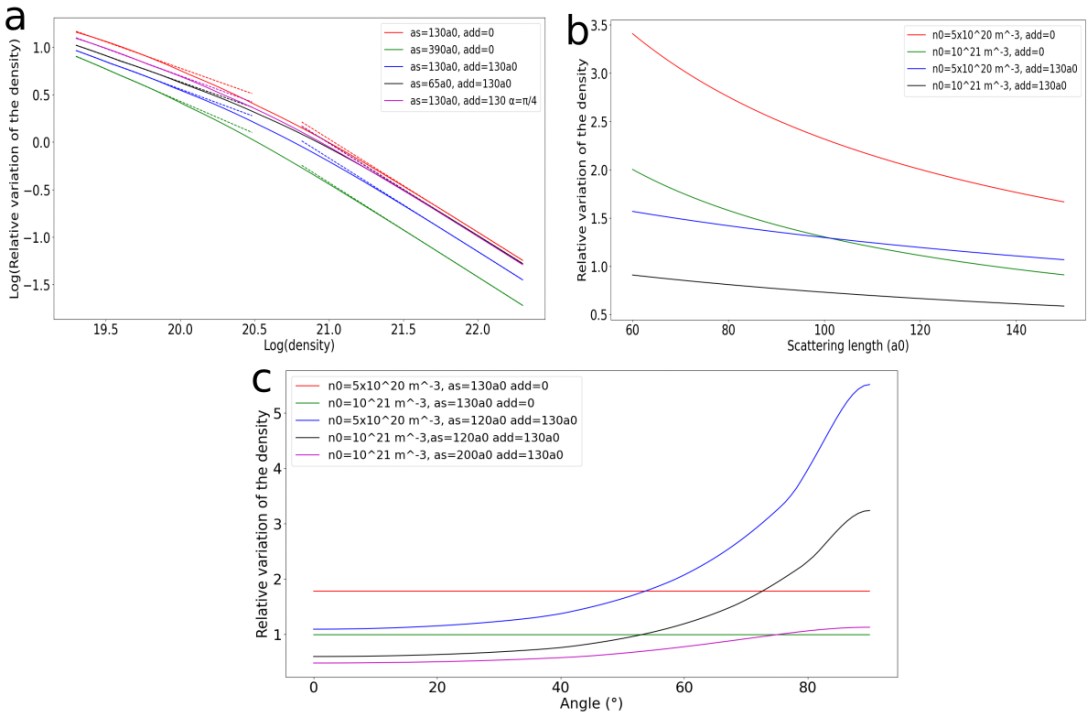


FIGURE 15 – Dependance of the perturbation of the density with the different parameters ($n_0$,$a_s$,$\alpha$). In all cases, the perturbation of the potential is generated with white noise for frequencies up to $4 \times 10^6$rad/m (**a**) Dependence with the background density in a log log scale. Except the line at $\alpha = \frac{\pi}{4}$, they are calculated at $\alpha = 0$. The perturbations clearly decreases with the density and two power law regimes seems to exist at low and high densities ; the dotted lines being the linear fit of these regimes. All the curves have approximately the same behavior but their starting values decreases as $a_s$ and $a_{dd}$ increases. Finally, for non zeros $\alpha$, the starting value increases and the transition between the two regimes seems faster. (**b**) Dependence with the s-wave scattering length. Except the line at $\alpha = \frac{\pi}{4}$, they are calculated at $\alpha = 0$. There is also a clear decrease of perturbation as $a_s$ increases and we recover the fact that the perturbation decrease with $n_0$ at fixed $a_s$ and $a_{dd}$. (**c**) Dependence with the angle of the dipoles with the vertical confinement direction. As expected, the purely contact case is constant, while in the other cases, tilting the dipoles increases the perturbations.

After this discussion, to get back to our original experimental question, using the best flat top potential obtained, with RMS deviation of 1.27% and a trap depth of $k_B \times 100$ nK, the variation of atomic density, for $n_0 = 10^{21}$ atoms/m$^3$, $a_{dd} = 133a_0$, $a_s = 130a_0$ and $\alpha = 0°$, is around 3% of $n_0$. Thus we can consider that the potential is flat enough to not be felt by the atomic cloud. The simulation of the atomic density is presented in Figure 16 (a), where the relative variation of the density is plotted for a potential perturbation shown in Figure 16 (b).

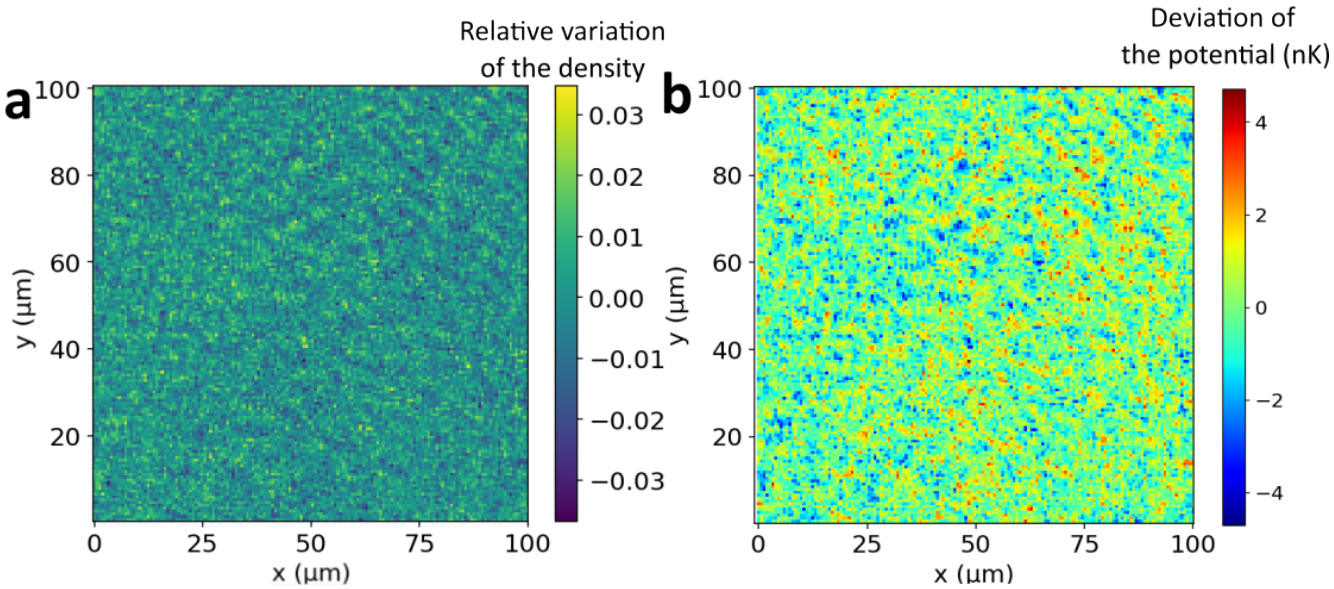


FIGURE 16 – (**a**) Simulation of the relative perturbation of the atomic density in a perturbed flat potential shown in (**b**). The mean value of the potential is $k_B \times 100$ nK$= 10^{-30}$J. The simulation is made for $n_0 = 10^{21}$ atoms/m$^3$, $a_{dd} = 133a_0$, $a_s = 130a_0$ and $\alpha = 0°$.

# Conclusion

Throughout this report we have demonstrated the possibility to create arbitrary potentials to trap atoms. The process of optimizing the trap geometry is reliable and stable enough to be used for several successive measurement runs ensuring the reproducibility of the experiment. Flat top with RMS deviation of 1.25% around the targeted intensity are obtained for trap 100µm wide. Simulations of the atomic cloud in these traps have shown that this will generate variation of the density of less than 3% which is probably good enough for the experiment.

Furthermore, not only flat top trap can be reached but also any kind of potential. It will be thus possible to study the behavior of dipolar gases of Dysprosium in a large variety of traps but also to induce any kind of velocity field in the cloud. Indeed, by projecting a non uniform potential on the atoms for a small amount of time $\tau$, the phase evolves as $-\frac{U(\mathbf{r})\tau}{\hbar}$ and so a phase gradient can be created. We can thus create for example vortices in the condensate with a phase winding potential.

Finally, it is now time to move the test setup to the main experiment but unfortunately some challenges will appears. Indeed, as we will not be able to image the final trap on the atoms, the light must be separated just before the final objective to be imaged (see Appendix) to optimize the trap. We hence need to hope that the imaged trap is as close as possible to the one on the atoms. Once a good enough flat top will be reached, it will probably be possible to optimize no longer with the image of the trap but with the density of the atoms.

# Appendices

## Polarizability calculations

We want to calculate the polarizability of Dysprosium to have the value of the potential trapping the atoms with equation (3). To do so, we need to express the scalar, vectorial and tensorial part of the polarizability from the spectroscopic data we have : the energy of the levels, labelled by their total angular momentum $J'$, their other quantum numbers $\beta'$ and their lifetime $\gamma_{\beta' J'}$. This is done using the equations of [9] :

$$\mathrm{Re}\left(\alpha_s\right) = \frac{2}{3\left(2J+1\right)} \sum_{\beta' \ J'} \frac{\left(E_{\beta' J'} - E_{\beta J}\right) \left|\langle \beta' \ J' || d || \beta \ J \rangle\right|^2}{\left(E_{\beta' J'} - E_{\beta J}\right)^2 - \hbar^2 \omega^2} \tag{15}$$

$$\mathrm{Im}\left(\alpha_s\right) = \frac{1}{3\left(2J+1\right)} \sum_{\beta' \ J'} \frac{\hbar \gamma_{\beta' J'} \left[\left(E_{\beta' J'} - E_{\beta J}\right)^2 + \hbar^2 \omega^2\right] \left|\langle \beta' \ J' || d || \beta \ J \rangle\right|^2}{\left[\left(E_{\beta' J'} - E_{\beta J}\right)^2 - \hbar^2 \omega^2\right]^2} \tag{16}$$

$$\mathrm{Re}\left(\alpha_v\right) = \sum_{\beta' \ J'} \frac{J'\left(J'+1\right) - J\left(J+1\right) - 2}{\left(J+1\right)\left(2J+1\right)} \times \frac{\hbar\omega \left|\langle \beta' \ J' || d || \beta \ J \rangle\right|^2}{\left(E_{\beta' J'} - E_{\beta J}\right)^2 - \hbar^2 \omega^2} \tag{17}$$

$$\mathrm{Im}\left(\alpha_v\right) = \sum_{\beta' \ J'} \frac{J'\left(J'+1\right) - J\left(J+1\right) - 2}{\left(J+1\right)\left(2J+1\right)} \times \frac{\hbar^2 \omega \gamma_{\beta' J'} \left(E_{\beta' J'} - E_{\beta J}\right) \left|\langle \beta' \ J' || d || \beta \ J \rangle\right|^2}{\left[\left(E_{\beta' J'} - E_{\beta J}\right)^2 - \hbar^2 \omega^2\right]^2} \tag{18}$$

$$\mathrm{Re}\left(\alpha_t\right) = -\sum_{\beta' \ J'} \frac{3\left[J'\left(J'+1\right) - J\left(J+1\right)\right]^2 - 9J'\left(J'+1\right) + J\left(J+1\right) + 6}{3\left(J+1\right)\left(2J+1\right)\left(2J+3\right)} \times \frac{\left(E_{\beta' J'} - E_{\beta J}\right) \left|\langle \beta' \ J' || d || \beta \ J \rangle\right|^2}{\left(E_{\beta' J'} - E_{\beta J}\right)^2 - \hbar^2 \omega^2} \tag{19}$$

$$\mathrm{Im}\left(\alpha_t\right) = -\sum_{\beta' \ J'} \frac{3\left[J'\left(J'+1\right) - J\left(J+1\right)\right]^2 - 9J'\left(J'+1\right) + J\left(J+1\right) + 6}{6\left(J+1\right)\left(2J+1\right)\left(2J+3\right)} \times \frac{\hbar \gamma_{\beta' J'} \left[\left(E_{\beta' J'} - E_{\beta J}\right)^2 + \hbar^2 \omega^2\right] \left|\langle \beta' \ J' || d || \beta \ J \rangle\right|^2}{\left[\left(E_{\beta' J'} - E_{\beta J}\right)^2 - \hbar^2 \omega^2\right]^2} \tag{20}$$

where $J = 8$ is the total angular momentum of the ground state of Dysprosium, $\beta$ the quantum numbers characterising this ground state. The sum is made only on the accessible states from the ground state, that is to say with $J' = 7, 8$ or $9$ because the light can only give 0, $\hbar$ or $-\hbar$ angular momentum to the atom.

We now need to express the reduced dipolar matrix element, this is done also with the equation of [9] :

$$\left|\langle \beta' \ J' || d || \beta \ J \rangle\right|^2 = \frac{3\pi\varepsilon_0 \hbar^4 c^3 \left(2J'+1\right) \gamma_{\beta' J'}}{\left(E_{\beta' J'} - E_{\beta J}\right)^3} \tag{21}$$

Let's now study the possibility to do a blue detuned trap between 600nm and 700nm. To do so, we need a negative part of the real polarizability : this happens only near resonances. In this range, there are 3 main resonances : $J \to J+1$ at 626nm, $J \to J-1$ at 657nm and $J \to J$ at 684nm.

Then like for the case at 532nm, the lifetime of the atoms is calculated and plotted in Figure 17 for different directions of the magnetic field and different polarization of light (linear in (a,b) and circular in (c,d). We see that the best lifetime is achieved at 657nm for a circular polarization. However, this lifetime

varies a lot with the direction of the magnetic field. It is hence better to use linear polarization : even if the lifetime is twice shorter, it is still of more than 100s, long enough for any experiment, and have the advantage to not depends on the direction of the field, making the alignment easier.

The best choice to have a blue detuned trap is then at 657nm with a light polarization along $y$ for a propagation along $z$ and a magnetic field in the $(x, z)$ plane.

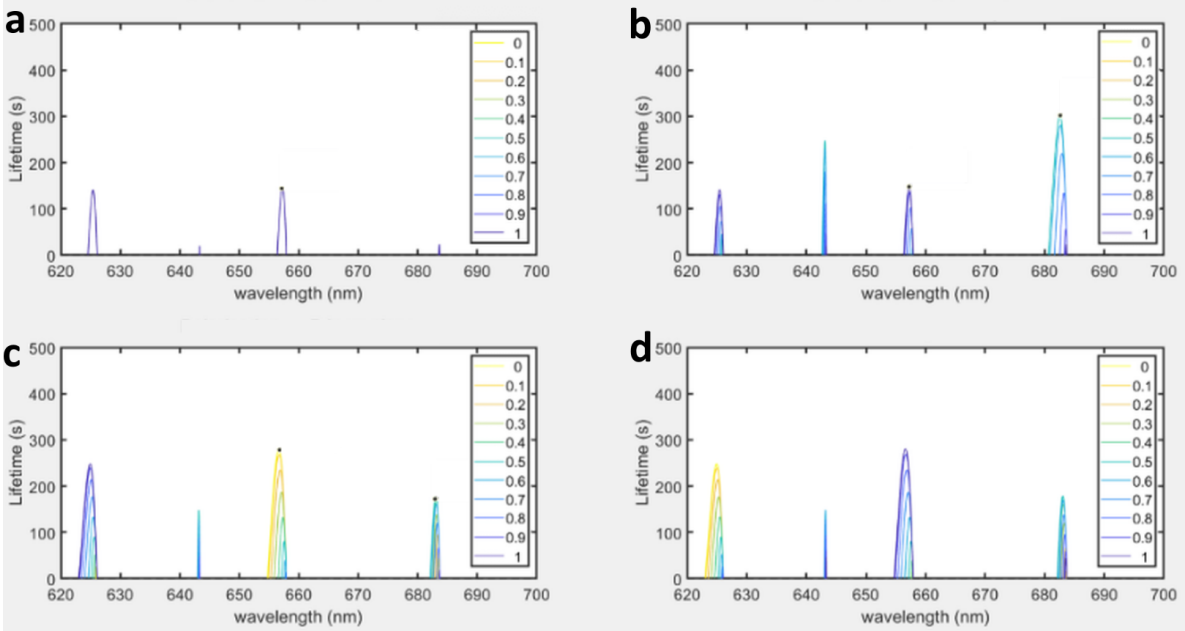


FIGURE 17 – Lifetime of Dysprosium atoms in a trap of depth 100 nK $\times k_B$. Only the wavelength were the trap is blue detuned are plotted. The light propagates along $z$ direction and the magnetic field is in the $(x, z)$ plane. The different curves are labelled by their angle with respect to $z$ in unit of $\pi$. (**a**) The polarization of light is linear and along $y$. There is no variation with the direction of the field and the resonance at 684nm is almost not visible. (**b**) The polarization of light is along $x$. The resonance at 684nm allows to have long life time if the angle is of $\pi/2$, indeed in that case the light is $\pi$ polarized and so we have a good probability for the transition $J \to J$. But it varies a lot when the magnetic field is tilted. (**c**) The light is $\sigma_+$ polarized, and here the transition $J \to J+1$ and $J \to J-1$ are enhanced. The $\sigma_-$ case in (**d**) is the same but by changing $\theta \to \pi - \theta$.

## Final setup

On the main experiment, the optical setup is almost unchanged but will differ from the test setup by mainly two things : first the Special Optics objective will be used. Its effective focal length is of 32.2mm, so to keep a demagnification of the same order as the test setup the lens of the second telescope is replaced by one with focal length of 501.8mm. The total demagnification is then of 78. Second it will not be possible to image the final trap, so the beam must be separated before the objective. This is done using a polarization beam splitter just before the objective. Furthermore, to project the image another lens must be used to complete the second 4f setup. This is done with a 175mm lens giving a total demagnification of 14.4. A small microscope objective will also be used to magnify the image on the camera. The setup is sketched to scale in Figure 18.

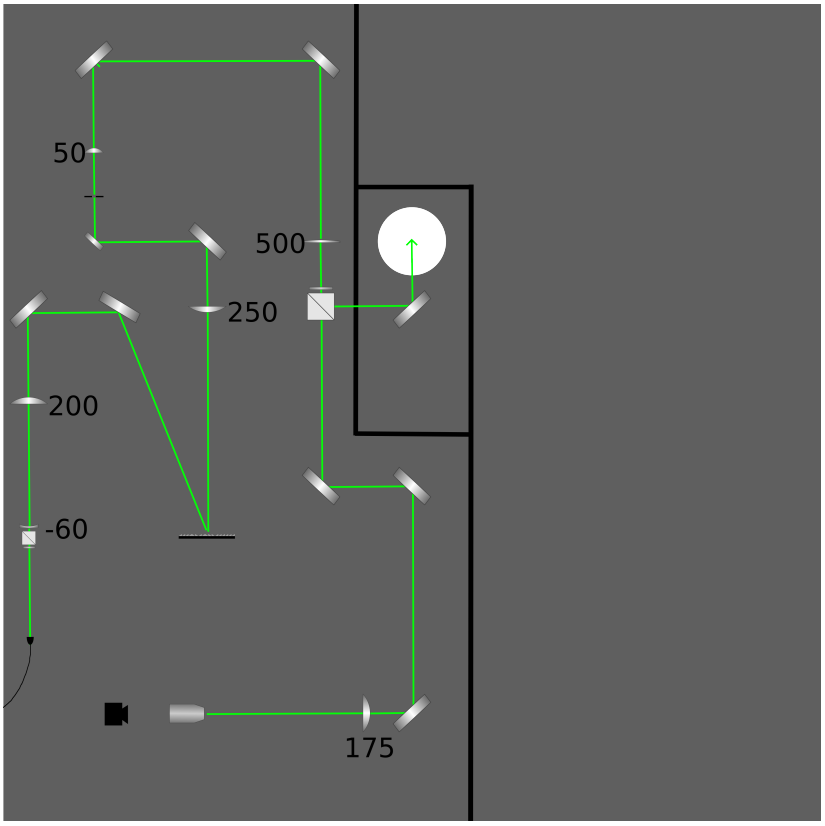


FIGURE 18 – Sketch of the setup that will be implemented on the main experiment. The beam is separated with a beam splitter cube just before entering the objective placed below the hole in the breadboard. On the transmission path of the cube, we have a lens, microscope objective and camera to image the trap we create. On the reflexion side, a mirror (not represented here) is positionned just above the hole of the breadboard to send the light to the Special Optics objective 200mm below. The right side of the breadboard is not used since it will be needed for another optical setup.

Finally the whole setup will be placed on a breadboard above the chamber and the light will enter the objective from above as shown in Figure 2 to trap the atoms in the horizontal plane, orthogonal to the direction of confinement of the accordion lattice.

## Detailled calculations of the GPE perturbations

We want to find the ground state of the atoms in the perturbed potential $V = V_0 + \delta V$. So we will start with the time independent version Gross Pitaevskii equation for quasi 2D dipolar gases (8) :

$$\mu\psi = \left[-\frac{\hbar^2}{2m}\nabla^2 + V\left(\overrightarrow{\rho}\right) + \frac{4\pi\hbar^2 a_s}{\sqrt{2\pi}ml_z}|\psi|^2 + \Phi_{dd}\right]\psi \tag{22}$$

If there were only contact interactions, the healing length of the system would be $l_h = \sqrt{\frac{\hbar^2}{mn_0\frac{4\pi\hbar^2 a_s}{m}}} \simeq$ 0.1µm for $10^{21}$ atoms/m$^3$, which is way smaller than the size of our trap of around 100µm. Thus we will neglect the variations of density at the border and check at the end that this is still true for dipolar gases. We develop then the wave function and chemical potential at first order :

$$\left\{\begin{array}{rcl}\psi &=& \sqrt{n_0 l_z} + \psi^{(1)} \\ \mu &=& \mu^{(0)} + \mu^{(1)}\end{array}\right. \tag{23}$$

Injecting into the equation (22), and keeping only order 0, we get :

$$\mu_0\sqrt{n_0 l_z} = V_0\sqrt{n_0 l_z} + \frac{4\pi\hbar^2 a_s}{m\sqrt{2\pi}l_z}n_0 l_z\sqrt{n_0 l_Z} + n_0 l_z\sqrt{n_0 l_z}\int_{trap} U_{dd}^{2D}\left(\overrightarrow{\rho} - \overrightarrow{\rho}'\right)\mathrm{d}\overrightarrow{\rho}' \tag{24}$$

Since we neglected the border sections, all the atoms are surrounded by roughly the same number of atoms and since $U_{dd}^{2D}$ scales as $\frac{1}{r^3}$, we can neglect the finite size effect and assume that the integral in (24) is taken over the whole space :

$$\int_{trap} U_{dd}^{2D}\left(\overrightarrow{\rho} - \overrightarrow{\rho}'\right)\mathrm{d}\overrightarrow{\rho}' \simeq \int_{\mathbb{R}^2} U_{dd}^{2D}\left(\overrightarrow{\rho} - \overrightarrow{\rho}'\right)\mathrm{d}\overrightarrow{\rho}' = \mathcal{F}\left(U_{dd}^{2D}\right)\left(\overrightarrow{0}\right)$$

So with the expression of the Fourier transform of the 2D dipolar potential (10), we get :

$$\mu^{(0)} = V_0 + \frac{4\pi\hbar^2 a_s}{m\sqrt{2\pi}m}n_0 + \frac{\mu_0\mu_m^2}{3\sqrt{2\pi}}n_0\left[-\sin^2\alpha + 2\cos^2\alpha\right]$$

We can change the origin of the energy to remove $V_0$, and rewrite the potential with $\varepsilon_{dd} = \frac{m\mu_0\mu_m^2}{12\pi a_s\hbar^2}$ :

$$\mu^{(0)} = \frac{4\pi\hbar^2 a_s}{m\sqrt{2\pi}m}n_0\left[1 + \varepsilon_{dd}\left(3\cos^2\alpha - 1\right)\right] \tag{25}$$

Let's now go to first order with still $V_0 = 0$ :

$$\begin{aligned}\mu^{(0)}\sqrt{n_0 l_z} + \mu^{(0)}\psi^{(1)} + \mu^{(1)}\sqrt{n_0 l_z} = \delta V\sqrt{n_0 l_z} - \frac{\hbar^2}{2m}\nabla_\rho^2\psi^{(1)} + \frac{4\pi\hbar^2 a_s}{m\sqrt{2\pi}l_Z}\left(\sqrt{n_0 l_z}\psi^{(1)} + \sqrt{n_0 l_z}\psi^{*(1)} + n_0 l_z\right) \\ + \left[\sqrt{n_0 l_z} + \psi^{(1)}\left(\overrightarrow{\rho}\right)\right]\int U_{dd}^{2D}\left(\overrightarrow{\rho} - \overrightarrow{\rho}'\right)\left[\sqrt{n_0 l_z}\psi^{(1)}\left(\overrightarrow{\rho}'\right) + \sqrt{n_0 l_z}\psi^{*(1)}\left(\overrightarrow{\rho}'\right) + n_0 l_z\right]\mathrm{d}\overrightarrow{\rho}'\end{aligned}$$

The zeroth order simplifies and we get, keeping only order 1 terms :

$$\begin{aligned}\mu^{(0)}\psi^{(1)} + \mu^{(1)}\sqrt{n_0 l_z} = \delta V\sqrt{n_0 l_z} - \frac{\hbar^2}{2m}\nabla_\rho^2\psi^{(1)} + \frac{4\pi\hbar^2 a_s}{m\sqrt{2\pi}l_z}\left(2n_0 l_z\psi^{(1)} + n_0 l_z\psi^{*(1)}\right) \\ + n_0 l_z\psi^{(1)}\int U_{dd}^{2D}\left(\overrightarrow{\rho} - \overrightarrow{\rho}'\right)\mathrm{d}\overrightarrow{\rho}' + n_0 l_z\int U_{dd}^{2D}\left(\overrightarrow{\rho} - \overrightarrow{\rho}'\right)\left[\psi^{(1)}\left(\overrightarrow{\rho}'\right) + \psi^{*(1)}\left(\overrightarrow{\rho}'\right)\right]\mathrm{d}\overrightarrow{\rho}'\end{aligned}$$

The expression of the order 0 of the chemical potential (25) appears in factor of $\psi^{(1)}$ and simplifies the equation into :

$$\mu^{(1)}\sqrt{n_0 l_z} = \delta V\sqrt{n_0 l_z} - \frac{\hbar^2}{2m}\nabla_\rho^2\psi^{(1)} + \frac{4\pi\hbar^2 a_s}{m\sqrt{2\pi}} n_0 \left(\psi^{(1)} + \psi^{*(1)}\right) + n_0 l_z \int U_{dd}^{2D}\left(\overrightarrow{\rho} - \overrightarrow{\rho}'\right)\left[\psi^{(1)}\left(\overrightarrow{\rho}'\right) + \psi^{*(1)}\left(\overrightarrow{\rho}'\right)\right] \mathrm{d}\overrightarrow{\rho}' \tag{26}$$

It is now time to go to Fourier space :

$$\left\{\begin{array}{rcl} \psi^{(1)} & = & \displaystyle\sum_{\overrightarrow{k}} \psi_{\overrightarrow{k}}\ e^{i\overrightarrow{k}\cdot\overrightarrow{\rho}} \\ \delta V & = & \displaystyle\sum_{\overrightarrow{k}\neq 0} \delta V_{\overrightarrow{k}}\ e^{i\overrightarrow{k}\cdot\overrightarrow{\rho}} \end{array}\right. \tag{27}$$

The potential perturbation has no $\overrightarrow{k} = 0$ component since it has zero mean. Furthermore, since we look for an equilibrium state, the chemical potential is uniform : $\mu^{(1)}$ is not developped over Fourier modes.

Injecting this in the equation (26), we get :

$$\begin{aligned}\mu^{(1)}\sqrt{n_0 l_z} = \sqrt{n_0 l_z}\sum_{\overrightarrow{k}\neq 0}\delta V_{\overrightarrow{k}}\ e^{i\overrightarrow{k}\cdot\overrightarrow{\rho}} + \frac{\hbar^2}{2m}\sum_{\overrightarrow{k}} k^2\ \psi_{\overrightarrow{k}}\ e^{i\overrightarrow{k}\cdot\overrightarrow{\rho}} + \frac{4\pi\hbar^2 a_s}{m\sqrt{2\pi}} n_0 \sum_{\overrightarrow{k}}\left(\psi_{\overrightarrow{k}} + \psi^*_{-\overrightarrow{k}}\right)\ e^{i\overrightarrow{k}\cdot\overrightarrow{\rho}} \\ + n_0 l_z \sum_{\overrightarrow{k}}\int U_{dd}^{2D}\left(\overrightarrow{\rho} - \overrightarrow{\rho}'\right)\left(\psi_{\overrightarrow{k}} + \psi^*_{-\overrightarrow{k}}\right)\ e^{i\overrightarrow{k}\cdot\overrightarrow{\rho}}\mathrm{d}\overrightarrow{\rho}'\end{aligned} \tag{28}$$

The term of zero frequency is then :

$$\mu^{(1)}\sqrt{n_0 l_z} = \frac{4\pi\hbar^2 a_s}{m\sqrt{2\pi}m} n_0 \left(\psi_{\overrightarrow{0}} + \psi^*_{\overrightarrow{0}}\right) + n_0 l_z \left(\psi_{\overrightarrow{0}} + \psi^*_{\overrightarrow{0}}\right)\int U_{dd}^{2D}\left(\overrightarrow{\rho} - \overrightarrow{\rho}'\right)\mathrm{d}\overrightarrow{\rho}'$$

So :

$$\mu^{(1)}\sqrt{n_0 l_z} = \left[\frac{4\pi\hbar^2 a_s}{m\sqrt{2\pi}m} n_0 + n_0 \frac{4\pi\mu_0\mu_m^2}{9\sqrt{2\pi}}\left(3\cos^2\alpha - 1\right)\right]\left(\psi_{\overrightarrow{0}} + \psi^*_{\overrightarrow{0}}\right)$$

Since the total number of atoms is not modified by the perturbation, we have $\left\langle\psi^{(1)}\right\rangle = 0$, that is to say $\psi_{\overrightarrow{0}} = 0$. Thus the first order of the chemical potential vanishes : $\mu^{(1)} = 0$ !

Let's now look at the non zero frequencies, we have :

$$0 = \left[\sqrt{n_0 l_z}\delta V_{\overrightarrow{k}} + \frac{\hbar^2}{2m}k^2\psi_{\overrightarrow{k}}\right]\ e^{i\overrightarrow{k}\cdot\overrightarrow{\rho}} + \left[\frac{4\pi\hbar^2 a_s}{m\sqrt{2\pi}} n_0 e^{i\overrightarrow{k}\cdot\overrightarrow{\rho}} + n_0 l_z\ e^{i\overrightarrow{k}\cdot\overrightarrow{\rho}}\int U_{dd}^{2D}\left(\overrightarrow{\rho} - \overrightarrow{\rho}'\right)\ e^{-i\overrightarrow{k}\cdot\left(\overrightarrow{\rho}-\overrightarrow{\rho}'\right)}\mathrm{d}\overrightarrow{\rho}'\right]\left(\psi_{\overrightarrow{k}} + \psi^*_{-\overrightarrow{k}}\right)$$

We see that the Fourier transform of the 2D dipolar interaction appears, whose expression is given in (10), and so we get :

$$0 = \sqrt{n_0 l_z}\delta V_{\overrightarrow{k}} + \frac{\hbar^2}{2m}k^2\psi_{\overrightarrow{k}} + \left[\frac{4\pi\hbar^2 a_s}{m\sqrt{2\pi}} n_0 + \frac{\mu_0\mu_m^2}{3\sqrt{2\pi}l_z}\left(F_\parallel\left(\overrightarrow{q}\right)\sin^2\alpha + F_\perp\left(\overrightarrow{q}\right)\cos^2\alpha\right)\right]\left(\psi_{\overrightarrow{k}} + \psi^*_{-\overrightarrow{k}}\right) \tag{29}$$

We denote $\lambda\left(\overrightarrow{k}\right) = \frac{4\pi\hbar^2 a_s}{m\sqrt{2\pi}} n_0 + \frac{\mu_0\mu_m^2}{3\sqrt{2\pi}l_z}\left(F_\parallel\left(\overrightarrow{q}\right)\sin^2\alpha + F_\perp\left(\overrightarrow{q}\right)\cos^2\alpha\right)$ and writing (29) for $\overrightarrow{k}$ and $-\overrightarrow{k}$, we get :

$$\left\{\begin{array}{rcl} -\sqrt{n_0 l_z}\delta V_{\overrightarrow{k}} & = & \left[\frac{\hbar^2}{2m}k^2 + \lambda\left(\overrightarrow{k}\right)\right]\psi_{\overrightarrow{k}} + \lambda\left(\overrightarrow{k}\right)\psi^*_{-\overrightarrow{k}} \\ -\sqrt{n_0 l_z}\delta V^*_{-\overrightarrow{k}} & = & \left[\frac{\hbar^2}{2m}k^2 + \lambda\left(-\overrightarrow{k}\right)\right]\psi^*_{-\overrightarrow{k}} + \lambda\left(-\overrightarrow{k}\right)\psi_{\overrightarrow{k}} \end{array}\right.$$

Since the perturbation of the potential is real, we have $\delta V^*_{-\overrightarrow{k}} = \delta V_{\overrightarrow{k}}$. It is then possible to equate these two equations and to get :

$$\psi_{\overrightarrow{k}} \left[ \frac{\hbar^2}{2m} k^2 + \lambda\left(\overrightarrow{k}\right) - \lambda\left(-\overrightarrow{k}\right) \right] = \psi^*_{-\overrightarrow{k}} \left[ \frac{\hbar^2}{2m} k^2 + \lambda\left(-\overrightarrow{k}\right) - \lambda\left(\overrightarrow{k}\right) \right]$$

But looking at the expressions of $F_{\parallel,\perp}$ (11), we see that they don't depend on the sign of $\overrightarrow{k}$ and so $\lambda\left(\overrightarrow{k}\right) - \lambda\left(-\overrightarrow{k}\right) = 0$. So we get : $\psi_{\overrightarrow{k}} = \psi^*_{-\overrightarrow{k}}$ ! This allows us to directly link the perturbation of the wavefunction with the one of the potential with (29) :

$$-\sqrt{n_0 l_z}\delta V_{\overrightarrow{k}} = \left[ \frac{\hbar^2}{2m} k^2 + 2\lambda\left(\overrightarrow{k}\right) \right] \psi_{\overrightarrow{k}}$$

Using the expressions of $\lambda\left(\overrightarrow{k}\right)$ and $F_{\parallel,\perp}$, we finally have :

$$\boxed{\psi_k = \frac{-\sqrt{n_0 l_z}}{\frac{\hbar^2 k^2}{2m} + 2 \times \frac{4\pi\hbar^2 a_s}{m\sqrt{2\pi}} n_0 \left[ 1 + \varepsilon_{dd} \left( 3\cos^2\alpha - 1 + 3\sqrt{\pi}\frac{q_x^2}{q} e^{q^2} \mathrm{erfc}\left(q\right) - 3\sqrt{\pi} e^{q^2} \mathrm{erfc}\left(q\right) \left( \frac{q_x^2}{q} + q \right) \cos^2\alpha \right) \right]} \delta V_k} \tag{30}$$

# References


[1] L. Chomaz, I. Ferrier-Barbut, F. Ferlaino, B. Laburthe-Tolra, B. L. Lev, and T. Pfau. Dipolar physics : a review of experiments with magnetic quantum gases. *Rep. Prog. Phys.*, 86 :026401, Dec 2022.

[2] S. Stringari L. Pitaevskii. *Bose Einstein condensation and superfluidity.* Clarendon press, 2003.

[3] Berezinskii. Destruction of long-range order in one-dimensional and two-dimensional systems having a continuous symmetry group i. classical systems. *Sov. Phys. JETP*, 32(3) :493–500, 1971.

[4] J. Schöner. Magnetic-field setup for magneto-optical-trapping and interaction-tuning in novel dysprosium quantum gas experiment. Master's thesis, Heidelberg University, 2022.

[5] P. Holzenkamp. An optical dipole trap with tunable geometry for dysprosium. Bachelor's thesis, Heidelberg University, 2022.

[6] V. Salazar Silva. The accordion lattice . toward trapping of dysprosium ultracold gases in two dimensions. Master's thesis, Heidelberg University, 2023.

[7] Rudolf Grimm, Matthias Weidemüller, and Yurii B. Ovchinnikov. Optical dipole traps for neutral atoms. volume 42 of *Advances In Atomic, Molecular, and Optical Physics*, pages 95–170. Academic Press, 2000.

[8] J. H. Becher, S. Baier, K. Aikawa, M. Lepers, J.-F. Wyart, O. Dulieu, and F. Ferlaino. Anisotropic polarizability of erbium atoms. *Phys. Rev. A*, 97 :012509, Jan 2018.

[9] Hui Li, Jean-François Wyart, Olivier Dulieu, and Maxence Lepers. Anisotropic optical trapping as a manifestation of the complex electronic structure of ultracold lanthanide atoms : The example of holmium. *Phys. Rev. A*, 95 :062508, Jun 2017.

[10] M. Schmitt. *A Self-bound Dilute Quantum Liquid of Dysprosium Atoms.* PhD thesis, Fakultät Mathematik und Physik der Universit¨at Stuttgart, 2017.

[11] Sébastien M. Popoff, Gilbert Shih, Dirk B., and GustavePariente. wavefrontshaping/alp4lib : 1.0.1, February 2022.

[12] G. B. Airy. On the diffraction of an object-glass with circular aperture. *Transactions of the Cambridge Philosophical Society*, 5 :283–291, 1835.

[13] BAYER B. E. An optimum method for two-level rendition of continuous-tone pictures. *Ineternl. Conf. On Comm.*, 50 :69–77, 1976.

[14] FLOYD R. W. An adaptive algorithm for spatial gray-scale. *Proc. Soc. Inf. Disp.*, 17 :75–77, 1976.

[15] Becker MF. Heinzen DJ. Liang J., Kohn RN Jr. 1.5% root-mean-square flat-intensity laser beam formed using a binary-amplitude spatial light modulator. *Applied Optics*, 48 :1955–1962, April 2009.

[16] Maxime Bocher. Introduction to the theory of fourier's series. *Annals of Mathematics*, 7(3) :81–152, 1906.

[17] Péter Juhász, Milan Krstajić, David Strachan, Edward Gandar, and Robert P. Smith. How to realize a homogeneous dipolar bose gas in the roton regime. *Phys. Rev. A*, 105 :L061301, Jun 2022.

[18] Sébastien M. Popoff. About mechanical stability using Vialux DMDs. `https://www.wavefrontshaping.net/post/id/25`.

[19] Christopher Ticknor, Ryan M. Wilson, and John L. Bohn. Anisotropic superfluidity in a dipolar bose gas. *Phys. Rev. Lett.*, 106 :065301, Feb 2011.

[20] L. Santos, G. V. Shlyapnikov, and M. Lewenstein. Roton-maxon spectrum and stability of trapped dipolar bose-einstein condensates. *Phys. Rev. Lett.*, 90 :250403, Jun 2003.